2017-01-01

Design Optimization For Heat Dissipation In Polymer Additive Manufacturing With Joule Heating

Tania Alejandra Ventura
University of Texas at El Paso, taventuraluna@miners.utep.edu

DESIGN OPTIMIZATION FOR HEAT DISSIPATION IN POLYMER ADDITIVE MANUFACTURING WITH JOULE HEATING

TANIA ALEJANDRA VENTURA LUNA

Master's Program in Mechanical Engineering

APPROVED:

Jack F. Chessa, Ph.D., Chair

Calvin M. Stewart, Ph.D.

Bill Tseng, Ph.D.

Charles Ambler, Ph.D.
Dean of the Graduate School

Dedication

A mis padres, Raúl y Rosa por ser el pilar fundamental en todo lo que soy, en toda mi educación, tanto académica, como de la vida. Mis hermanas, Julieta y Grisel por su incondicional apoyo mantenido a través del tiempo y la distancia. Los quiero mucho.

Todo este trabajo ha sido posible gracias a ellos.

DESIGN OPTIMIZATION FOR HEAT DISSIPATION IN POLYMVER ADDITIVE MANUFACTURING WITH JOULE HEATING

by

TANIA ALEJANDRA VENTURA LUNA, B.S in Mechanical Engineering

THESIS

Presented to the Faculty of the Graduate School of

The University of Texas at El Paso

in Partial Fulfillment

of the Requirements

for the Degree of

MASTER OF SCIENCE

Department of Mechanical Engineering

THE UNIVERSITY OF TEXAS AT EL PASO

May 2017

Acknowledgements

First, I would like to express my sincere gratitude to my advisor, Dr. Jack F. Chessa, for the continuous support, patience and motivation during my Master studies. Thank you for teaching me and sharing a small part of your great knowledge, it was an honor being your student.

Besides my advisor, I would like to thank Dr. Calvin Stewart and Dr. Bill Tseng for accepting to be part of my committee. Foremost, I would like to thank W.M. Keck Center for 3D innovation Laboratory, especially to David Espalin, for giving me the opportunity to contribute to the amazing technology of additive manufacturing.

My sincere thanks to Dr. Luis Echegoyen for giving me the opportunity to use the equipment from his chemistry laboratory and Elkin Romero for his assistance to teach me how to use high temperature furnaces.

I thank my lab mates at the University of Texas at El Paso, Gerardo Reyes, Carlos Garcia, Alejandra Cabral, Raudel Avila, Eduardo Garcia, Alan Esparza, Luis Chavez, Jorge Silva, Shafinul Haque, and Quetzalcoatl Mendoza, for all their support and for making enjoyable all mornings, afternoons and late nights. I thank my friends, Andrea, Genesis, Joanna, Monica, Brenda, Salvador, Vivian and Gilbert, thank you for a friendship that lasts despite distance.

Also, I would like to thank my parents, Raúl and Rosa and my sisters Julieta and Grisel for supporting me throughout my life.

Last, but not least, I would like to thank José Luis, who has been a constant source of support and encouragement, I thank you for always being my best friend.

Abstract

Nowadays, the use of additive manufacturing (AM) is mainly focused on the production of prototypes with the purpose of evaluating a design. This industry has become a subject of constant reinvention; in fact, an emerging application of AM is focused on creating parts with embedded electronics. However, the development of both traditional and additive manufactured electronics has led to an increase in power densities and size reduction. Consequently, thermal management has become essential in electronics, as overheating decreases reliability of the component leading to a premature failure.

In this study, a polycarbonate component design with integral electrical circuitry that is fabricated by Material Extrusion process is considered. In addition to copper deposited in the Material Extrusion process for the circuitry, complementary copper is deposited to help conduct the heat generated by the joule effect.

The focus of this research is to optimize the placement of metal for heat conduction. A computational parametric design study was considered, by using Finite Element Analysis (FEA) that allowed the development of a design that models heat generation and temperature in the circuitry. In conjunction with the FEA, the development of Response Surface Methodology (RSM) and linear constrained optimization, assisted in the guidance to achieve a design optimization. This guided methodology optimized the model by effectively increasing heat dissipation through the additional copper wire. The optimized model with additional deposited copper wire dissipated 50.43% of the total heat generated, whereas, previous design dissipated only 9.49% of the total heat generated by the joule heating. In addition, temperature was lowered from 118.05 ℃ to 29.25 ℃ degrees. This concludes in an optimization of the heat dissipated through the additional deposited wires by 81.1%; and a decrease of the overall temperature component by 75.2%.

Table of Contents

List of Tables

List of Figures

1. Introduction

1.1 Additive Manufacturing

Additive manufacturing (AM) is the technology of joining materials by adding layer by layer of this, with the objective of creating three-dimensional (3D) objects. [1] This technique adds another form of manufacturing without the need for tools or molds. In contrast to traditional reductive methods such as milling or lathing which removes material to create a part, additive manufacturing works by sequentially adding more material to build up a part, reducing cost and time [2]. Additive manufacturing, also called rapid prototyping offers multiple advantages compare to traditional manufacturing such as: Manufacturing complex shapes and design flexibility, that otherwise it would be difficult due to the constraints that some traditional methods have. Allows the fast production of samples and reduction of error and cost. In other words, since parts are sketched in CAD, they can be easily corrected and modified before printing. Also, the fast and low-priced production of prototypes let designers to evaluate and provide feedback during the design process. By doing this, it becomes easier for engineers or designers to detect any error in the design such as tolerances, interfacing, among others prior the final manufacturing of the component.

Moreover, this technique has given the opportunity to provide not only prototypes but customizable and functional components. Initially, AM was used specifically to create visualization models for products as they were being developed. It is widely known that models can be much more helpful than drawings or renderings in fully understanding the intent of the designer when presenting the conceptual design [3]. Nevertheless, advances in AM has allow this technology to create functional components such as prosthetic and electrical components among others, providing all the advantages mentioned before.

1.2 Material Extrusion Process

As discussed in section 1.1 (AM) builds an object by piling layers of material until the object is finished. Rapid prototyping offers several techniques such as Material Extrusion process, stereolithography (SL), selective laser sintering (SLS), laminated object manufacturing (LOM) and 3D printing and solid ground curing (SGC). One of the most used techniques by extrusion is Material Extrusion process, where the part is built bottom up layer by layer by heating and extruding thermoplastic filament [4]. The process can be divided into the following:

Pre-Processing: To create objects with a (FDM) printer, a computer aided design (CAD) file and converted into a format that the 3D printer will be able to read *i.e.* .STL file.

Processing: FDM printers use two types of materials. The first one is the modeling thermoplastic filament material such as polycarbonate or (PLA), (ABS) or polycarbonate which constitutes the desired object and the second material is often called the support material. The second material acts like a scaffolding that supports the main object and later removed. During the printing process the material in form or filament goes out through and extrusion nozzle. The nozzle melts the filaments and extrudes them onto a base. Both the nozzle and the base are controlled by a computer that translates the dimensions of an object into X, Y and Z coordinates for the nozzle and base to follow during printing [5]. In a FDM system, the extrusion nozzle moves over the build platform horizontally and vertically, "drawing" a cross section of an object onto the platform. This thin layer of plastic cools and hardens, immediately binding to the layer beneath it. Once a layer is completed, the base is lowered to make room for the next layer of plastic [5].

Post Processing: After the FDM printer finished with an object is done, the support material mentioned above can be easily removed.

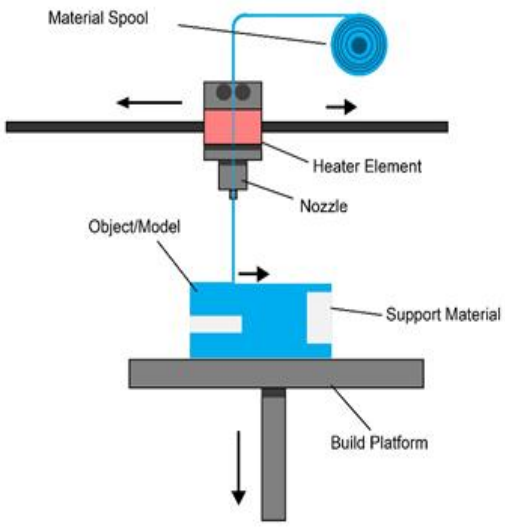

Figure 1.1: Material Extrusion process (Source: Loughborough University, 2017)

As previously indicated, the used of this advanced technology creates functional components, such as 3D printed electronics. Traditional electronics systems are usually fabricated via printed circuit boards (PCBs), which provide both the electrical interconnections between electronic components and the physical structures for mounting the components [6]. Nowadays, many applications particularly automotive, industrial systems, medical devices, consumer goods and aerospace, require high value, on-demand, fully functional electromechanical products with complex 3D structures, which creates challenges in the production of traditional PCB based electronics. Due to the manufacturing flexibility, hybrid additive manufacturing (AM) technology has been hailed to be a potential solution for this purpose [7]. Explained more in detail, hybrid additive manufacturing for electronics consists in printing polymers with embedded circuit wires. To achieve this, a combination of (FDM) additive manufacturing technique, and inkjet deposition are used to build integrated electrical components with wire embedding; where the wire is directly inserted into the 3D printed polymer [9].

1.3 3D Printed Electronic Challenges

Electronic circuitry can be defined as a conjunction of basic electrical elements *i.e.* resistors, capacitors, diodes, transistors among others. These elements are linked by wires with high thermal conductivity *i.e*. copper to allow the flow of electric current. Electrical elements are classified in two major categories: Active and Passive and both groups form a circuit [13]. Active components require electrical power to operate and they produce energy in form of voltage such as diodes and transistors. Passive components do not require energy to operate, they store energy instead (Capacitors) or they drop energy (Resistors).

As mentioned before, the integration of these elements, create a circuit, thus create electrical devices. The energy produced by an electrical device generates heat, an undesirable effect also called '*The Joule Heating Effect'*. Joule heating (also referred to as resistive or ohmic heating) describes the process where the energy of an electric current is converted into heat as it flows through a resistance [8]. This effect has the disadvantage in 3D printed embedded electronics of overheating or a rise in temperature above the operating temperature. Overheating causes premature mechanical and electronic failure, having consequently a decreased in the reliability of the component. When these devices are fully enclosed, overheating is a serious problem if they are not being actively cooled. Moreover, nowadays there have been a decrease in the size of electronic components. This has increase the complexity of manage thermal effect due to the increase of concentrated heat fluxes in small components. Excess heat can adversely affect the mechanical performance of parts, and for every 10° C increase in temperature, the average reliability of electronic components decreases by 50% [10]. Since electronics have multiple uses in automotive, industrial systems, medical devices, consumer goods and aerospace among others; it is crucial for these devices to have a good design that increase reliability. High power electrical and electronic components continue to have an increasing demand for higher power dissipation within a relatively confined space. To provide for such higher power dissipation requirements While remaining suitably compact, several levels of thermal management are usually required at the device, sub-assembly and component level [14].

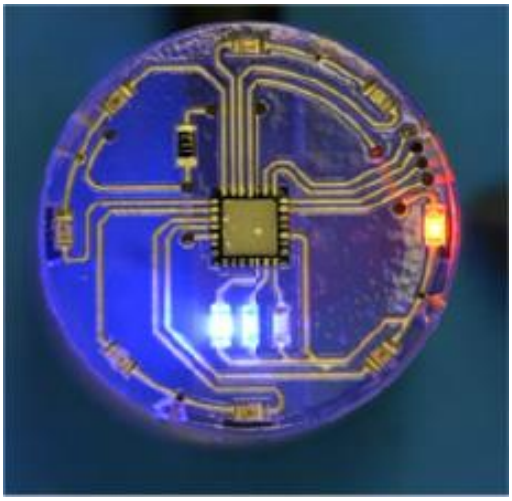

Figure 1.2: 3D Printed Electronic Component [49]

1.4 Literature review

In addition to complicated prototypes, additive manufacturing technology seeks to create functional components such as 3D printed embedded electronics. Researchers have attempt to address thermal management issue in traditional electronics, mainly through heat sinks, phase change material (PCM)-based cooling system and heat pipe cooling mechanisms [15]; [16]; [17]: [20]. Nonetheless, few research studies have been reported on overheating in the emerging technology of 3D printed embedded electronics. Nowadays, electronic designers pay much more attention to thermal design simply because they have no other choice. In the future, the two biggest constraints in the integration of electronics will be the removal of heat and interconnections. The reason behind the need for thermal modeling is increased power density in electronics [11].

Heat sinks, transfers energy from a higher temperature device to a lower temperature fluid. The fluid or medium is usually air, water or refrigerants. This form of heat exchanger increases heat dissipation by increasing the velocity of the fluid that flows through the fins. A heat sink can be classified in two groups: active and passive heat sinks. Active heat sinks require a power supply that are usually fan or peltier cooling device. Passive heat sinks do not have mechanical components and are made of aluminum-finned radiator that dissipates heat through convection

[12]. In an experimental investigation (Bhattacharyars and Mahajan, 2002) [17] heat dissipation in electronics was enhanced by incorporating fins in metal foam. Explained more in detail, finned metal foam heat sinks were investigated under forced convection with the intent of cooling electrical components. Investigation found that, that by adding more fins, the heat transfer coefficient increases as shown in Figure 1.3. However, when a certain number of fins are added, it retards heat transfer and the pressure drops due to the interference of thermal boundary layers.

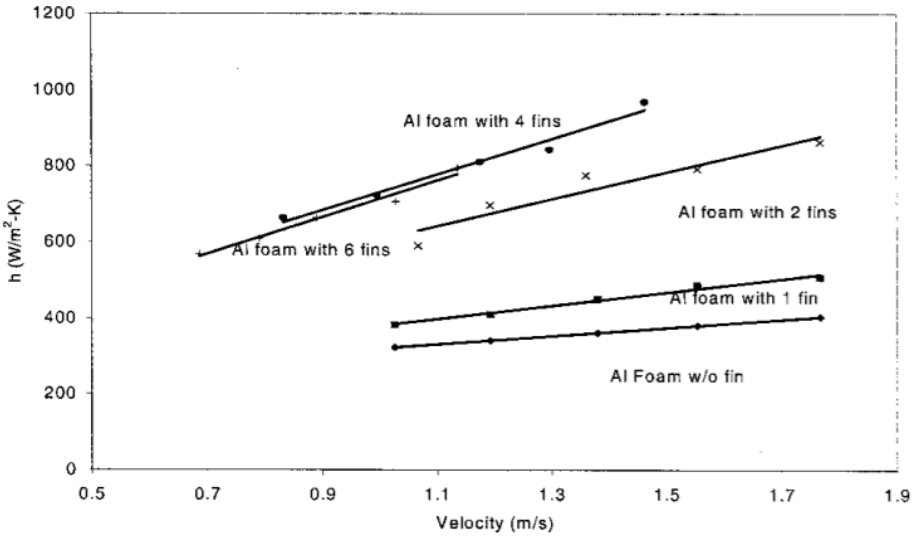

Figure 1.3: Heat Transfer coefficient as a function of velocity for the 20 PP1 foam Samples [17]

Another study (Gallego and Klett, 2003) [18] was done to investigate carbon foams for thermal management. High thermal conductivity carbon foam developed in Oak Ridge National Laboratory was used to create heat sinks and compare them with conventional heat sinks. Because of experimental work, it was demonstrated that, carbon foam is an efficient thermal management material. Compared with aluminum-based heat sinks, it was demonstrated that the foam-based heat sink can be used to reduce the volume of the cooling fluid required or potentially eliminate the water cooling system altogether [18]. (Escher et al., 2010) [19] presented an ultra-thin heat sink for electronics, combining optimized impinging slot-jets, micro-channels and manifolds for efficient cooling. Furthermore, it was demonstrated that the manifold system has a strong impact on the optimum choice of design parameters. Consequently, the overall performance of the heat

sink is determined by the interaction between the manifold dimensions and the heat transfer structure. (Escher et al., 2010) [19] demonstrate to have similar thermal resistance to previous investigations but with a design 20 times smaller than previous designs. Because of their work, investigation gave a maximum cooling capacity of 750 W/cm^2 for a temperature difference between fluid inlet and chip of 65 K [19].

Another cooling method for electronics with several performed studies and research is the heat pipe cooling mechanism. Heat pipes are used as a heat transfer device for applications such as electronics. Heat pipes dissipates heat through thermal conductivity and phase transition. At the hot interface within a heat pipe, which is typically at a very low pressure, a liquid in contact with a thermally conductive solid surface turns into a vapor by absorbing heat from that surface [16]. Heat pipe cooling of electronics has gain popularity due to the advantages that this system offers over heat sinks and pumped liquid cooling. Some of the advantages includes large equivalent thermal conductance, excellent packaging flexibility, passive operation and high reliability [20]. A study (Zuo, North et al., 2000) [15] discusses an advanced heat pipe mechanism capable of achieving heat fluxed over 250 W/cm^2. The mechanism utilizes thermally driven pulsating two-phase flow to achieve high heat flux capability and heat transfer coefficient. Moreover, after experimental work, it was concluded that pulsating heat pipes are feasible approaches to removing increasing heat dissipation densities in electronic equipment as shown below in Figure 1.4.

Mechanism	Heat Pipe Descriptions	Maximum q''	Thermal resistance
Conduction	Cu block	150 W/cm^2	0.933°C/W
Pulsating	60% fill ratio	175 W/cm^2	0.27°C/W
Pulsating	40% fill ratio	175 W/cm^2	0.58°C/W
Pulsating	50% fill ratio	160 W/cm^2	0.60°C/W
Pulsating	55% fill ratio	175 W/cm^2	0.30°C/W
Pulsating	60% fill ratio	175 W/cm^2	0.27°C/W
Pulsating	70% fill ratio	220 W/cm^2	0.16°C/W
Pulsating	80% fill ratio	185 W/cm^2	0.20°C/W

Figure 1.4: Prototype Pulsating Heat Pipe Test Results [15]

(Namba et al., 1998) [21] studied the performance of miniature heat pipes for cooling electronic equipment. Experiments for the miniature heat-pipe were conducted on their thermal properties and reliability. Miniature heat pipes with diameters ranging from 3 to 6 mm were designed for notebook computers. These heat pipes where used with a heat input of 15 W and maintaining a work temperature of 200 ℃. Results showed that after 10, 000 hours of operation heat pipes did no show degradation or corrosion; without the miniature heat pipes temperature, would have increase 10 degrees before 1000 hours of operation.

Lastly, another popular method for cooling is the use of phase change material (PCM)-based cooling system. This material is generally a substance that contains high heat of fusion, which is capable of store and release large amounts of energy when melting and solidifying occurs. Heat is absorbed or released when the material changes from solid to liquid and vice versa. Explained more in detail, when PCMs changes from solid to liquid it absorbs heat, that is why is widely used in electronic cooling [22]. As mentioned before, integrated circuits operate best within a limited temperature range; hence their packages must be designed to remove the excessive heat. As an alternative passive cooling technique means, PCMs have been widely investigated for such transient electronic cooling applications considering their advantages such as high latent heat of fusion, high specific heat, controllable temperature stability and small volume change during phase change, etc. [23]. Many researchers have widely investigated the PCM characteristics with the aim of improving the performance of electric cooling devices. (Weng et al., 2010) [20] experimentally investigated thermal performances of heat pipe with different phase change materials for cooling in electronics. Three kinds of PCMs including Lauric, Palmitic acids and Tricosane. These materials where analyze at different filling volumes, fans speed and heating powers. As a result of experimental validation, Tricosane showed to save up to 46% of the fan power and a drop-in temperature of 12.3 °C compare to thermal storage material. Figure 1.5 shows the temperature evolutions of different PCMs under the condition of various heating powers. As seen from the figures, Tricosane takes 973 s to reach 60°C at a heating power of 20W, but Lauric and Palmitic acids take 1041 and 582s to attain 60°C, respectively. At a heating power of 30W and 40W,

Tricosane needs 477 and 307s to achieve 60°C, respectively. Lauric acid takes 396 and 239s and palmitic acid needs 198 and 96s.

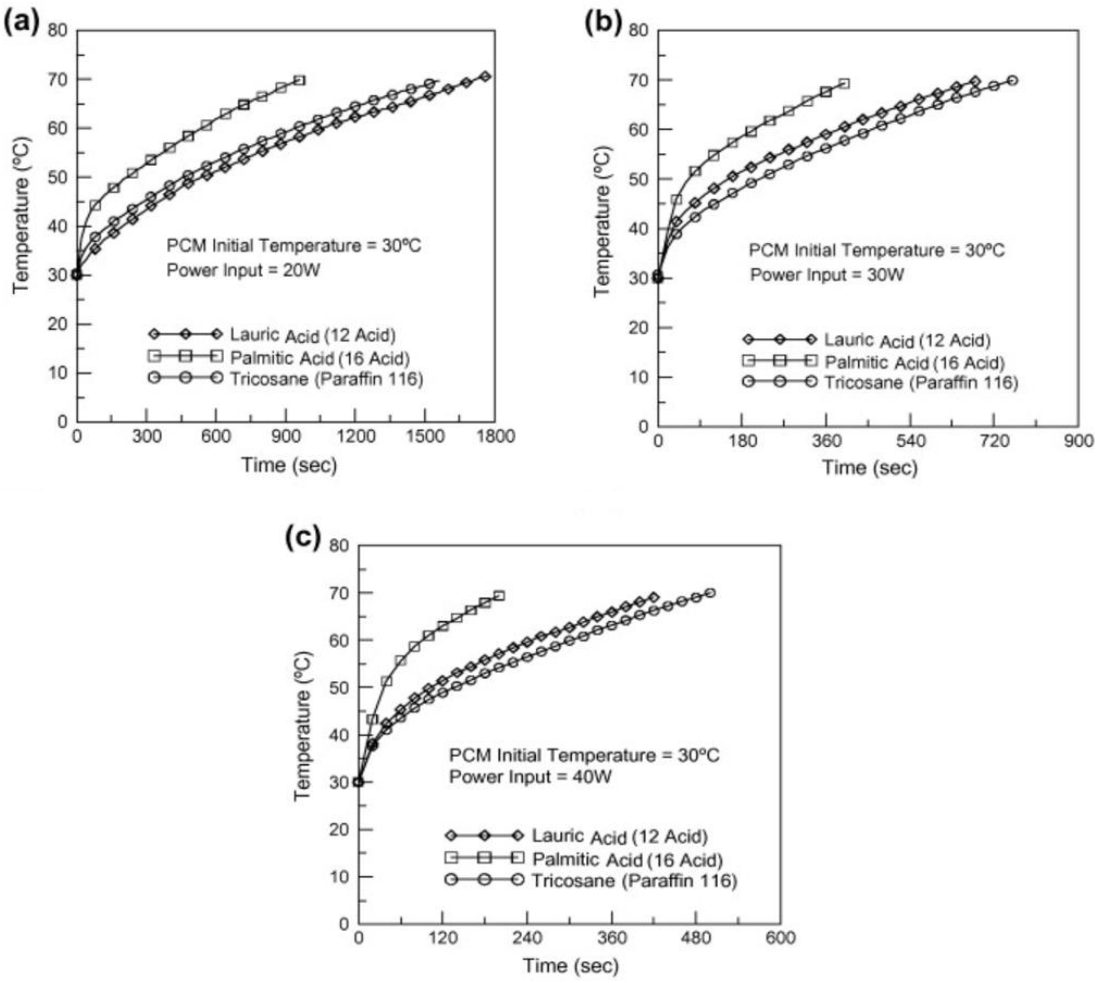

Figure 1.5: Heater temperature evolutions in different heating powers for Lauric acid, Palmitic acid and Tricosane, respectively: (a) 20W, (b) 30W, and (c) 40W [20]

Similarly, (Tan and Tso, 2004] [28] performed an experimental study to cool electronic devices such as mobiles, and wearable computers by using a heat storage unit (HSU) filled with phase change material (PCM) of n-eicosane inside the device. Experiments were performed to observe the temperature rise of the junction temperatures. Moreover, it was found that the use of HSU helps to stabilize the system temperature to an allowable working temperature of 50 °C.

Temperatures increases rapidly without the use of PCM in heat storage units. However, at high power dissipation, the junction temperature exceeds the working temperature.

As explained above, extensive research and studies have been performed to ensure reliability on electronics by maintaining them at a safe operating temperature. However, since additive manufacturing for electronics is relatively new, few research studies have been focus to cool 3D printed electronic components. Research explained above, showed cooling methods such as heat sinks, heating pipes and phase change material cooling system; nonetheless, few apply to additive manufacturing. Explained more in detail, heating pipes show a high potential for heat dissipation and electronic cooling; yet, it cannot be applied to additive manufacturing electronics since pipes cannot be embedded by Material Extrusion Process. For this reason, this research aims to provide another method of cooling electronics devices that is applicable for 3D printed electronic devices.

1.5 Thesis Motivation

Additive manufacturing offers infinite number of possibilities when creating new objects. This technology opens new, innovating and efficient ways of manufacturing; as it offers design flexibility, reduction in cost and time among other advantages. Nowadays, AM promises building not only complex prototypes but functional components. 3D printed electronics with embedded wires build by FDM gives the opportunity of integrating circuits into complicated structures.

However, thermal management is a problem that electronics face; the joule heating effect can cause the degradation or melting of the electrical devices causing the premature failure of the component. While technology continues to facilitate complexity in 3D printed electronics, few research has been implemented to reduce overheating and improve long term reliability. Owing to the need of increasing reliability in the electrical devices; my research motivation is to design, simulate and optimize a 3D printed component with embedded joule heating by incorporating additional deposited copper wire. The main purpose of the deposited metal will be to reduce the overall temperature of the component by extracting the heat generated by the electronic circuitry

through natural convection using Finite Element Analysis. This research is an effort to contribute to this promising technology that allows to create unimaginable objects at a low cost with the intent of improving life quality.

1.6 Thesis Structure

As mentioned in the abstract, the objective of this study is to optimize a polycarbonate component design with integral embedded electrical circuitry that is fabricated by Material Extrusion process. To achieve this, additional copper wire without electrical current is deposited to help conduct heat and lower the overall temperature of the component generated by the heating source wire. This thesis outline, will briefly explain chapter by chapter the process to achieve this design optimization of heat dissipation and temperature.

Chapter 1, discusses FDM process, as well as thermal management challenges in 3D printed electronics, literature review and thesis motivation. Subsequent chapter delineates the theory needed to calculate boundary conditions used in the FEA model developed in the following chapter. Then, chapter 3 discusses in detail the finite element method used. First the base model set up is explained including, model description, geometry, mesh, thermal simulation and results. After that, the set up for the new model with additional deposited copper wire is discussed, this comprises model description, geometry, mesh, simulation and the results obtained. From there, chapter 4, delineates in detail the process of optimizing the new model with additional copper wire, this chapter explains the methodology employed in detail at each model refinement. Then, the mathematical optimization employed and the MATLAB code created is explained in the last section of this chapter. In addition, chapter 5, discusses the results obtained at each model refinement and for the constrained optimization. Finally, chapter 6, summarizes findings, conclusions and proposes possible future work in the field.

2. Thermal Analysis using Analytical Method

2.1 Heat Transfer Analysis

Heat can be defined as *"The form of energy that can be transferred from one system to another as a result of temperature difference."* [24]. Both, thermodynamics and heat transfer studies and analyzes heat. However, heat transfer differs from thermodynamics since it studies the rate at which the energy is transferred from one system to another. In other words, while thermodynamics focuses in the amount of heat transfer as a system experiences a process to achieve equilibrium; heat transfer focuses on how long the process will take. It is known that, that when heat is conducted, it may contain the conversion of electrical, nuclear or chemical energy into thermal energy or heat. This conversion process it is known as heat generation [24].

2.1.1 Heat Generation

To dissipate heat generated in 3D printed electronic components, it is important to understand the process of heat generation. As discussed before, electronic components need to operate at low temperatures to ensure reliability. To safely and effectively remove heat from heat generation *i.e.* electronic circuits, the use of heat transfer concepts is fundamental to achieve this.

The temperature of a resistance wire rises rapidly when electric current passes through it. In other words, the electrical energy is being converted to heat. This is a common thermal energy generation process that involves the conversion from electrical to thermal energy in a current-carrying medium (Ohmic, or resistance or joule heating) [25].

In 3D-printed electronics, the most commonly used materials are thermoplastics such as ABS, PLA and PC. These thermoplastics have their own advantages: ABS filament offers harder and durable objects and can withstand temperatures over 100 degrees before it starts to soften known as glass transition temperature [29]. On the other hand, PLA is biodegradable since it is made from plant material, however, is harder yet more brittle and prone to break when bent; it has

a glass transition temperature of 60-65 degrees Celsius. Finally, PC has a higher impact strength than ABS and has a higher glass transition temperature of 147 degrees Celsius [30]. Table 2.1 shown below summarizes the strength and glass transition temperature of the most common thermoplastics used in 3D printed.

Thermoplastic	Ultimate Tensile Strength **(MPA)**	Glass transition temperature (℃)
PC	70	145-147
ABS	40	100-105
PLA	57.8	60-65

Table 2.1: Average ultimate tensile strength and glass transition temperatures of thermoplastics.

For this reason, polycarbonate (PC) was chosen as the material for the electronic device. It is expected, that polycarbonate will withstand better the heat generated by the embedded copper wire. In the following sections, it will be explained how the heat generated by the joule heating effect dissipates through convection. Moreover, how this research aims to dissipate heat through additional deposited wire to reduce the overall temperature in PC due to joule heating effect. Figure 2.1 shows geometry and dimensions of the electronic device compose of polycarbonate block with embedded copper wire. Dimensions are used to calculate body heat flux of copper wire in section 2.1.3.

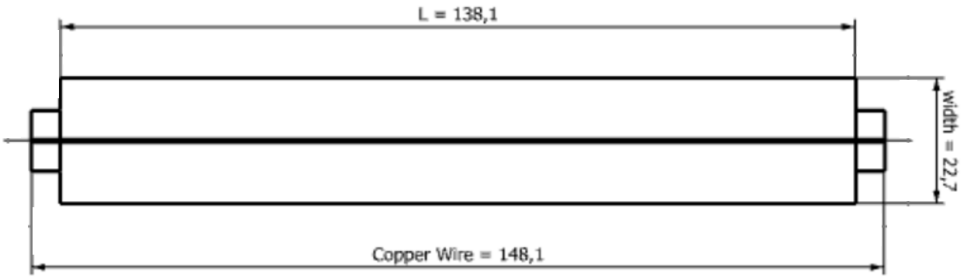

Figure 2.1: Dimensions of Polycarbonate block with embedded copper wire in mm.

2.1.2 Joule Heating

The power P absorbed in an electrical resistor of resistance R, current I, and voltage V is given by: $P = I^2 \cdot R = V^2/R = V \cdot I$. Even though it has units of power, it is commonly referred to as joule heat [26]. As mentioned in chapter 1, Joule heating, is also known as ohmic heating and resistive heating. The process is summarized as the passage of an electric current through a conductor to produce heat. Joule's first law, also known as the Joule–Lenz law, states that "*The power of heating generated by an electrical conductor is proportional to the product of its resistance and the square of the current*:" [28].

$$P \propto I^2 \cdot R \tag{2-1}$$

2.1.3 Body Heat Flux

The temperature of a medium increases during heat generation due to the absorption of the generated heat by the medium. As the temperature in the medium rises, the heat transfer does it too [24]. This will continue until steady condition is reached.

Heat generation or body heat flux is usually expressed per unit volume of medium, and is denoted by $\dot{\Delta}$, whose units are W/m^3. The heat generated by the copper wire of outer diameter d_o and length L to the electrical component can be expressed as

$$\dot{\Delta} = \frac{P}{V_{Wire}} = \frac{\varphi \cdot I^2}{\pi \cdot d^2/4} \qquad (W/m^3) \tag{2-2}$$

The rate at which energy is generated by passing a current ***I*** through a medium with electrical resistivity φ. To calculate total heat generated the following properties of copper from where used (see Table 2.2):

Table 2.2: Parameters used to calculate Heat Generation in copper wire.

Diameter ($\boldsymbol{d}$) $\boldsymbol{m}$	Radius ($\boldsymbol{r}$) $\boldsymbol{m}$	Length (l) $\boldsymbol{m}$	Area (A) $\boldsymbol{m^2}$	Current (I) **Amperes**	Copper wire resistivity ($\boldsymbol{\varphi}$) $\boldsymbol{\Omega \cdot m}$
$\boldsymbol{3.21e^{-4}}$	$1.605e^{-4}$	0.1381	$8.092e^{-8}$	5.5	$1.724e^{-8}$

First, power was calculated with the formula shown below where ΔV is the pressure drop and I is the current.

$$P = (\Delta V \cdot I) \tag{2-3}$$

Pressure drop is defined: R is the resistance and I is the current

$$\Delta V = I \cdot R \tag{2-4}$$

To calculate resistance the formula shown below is used. Where A represents the area of the copper wire φ is the resistivity of copper wire at a diameter of 0.321 mm and the total length is 0.1381 meters.

$$R = \varphi \cdot \frac{l}{A} \cdot I = 0.89 \qquad (W) \tag{2-5}$$

Power per unit length:

$$P = (\varphi \cdot \frac{l}{A}) \cdot I^2 = 6.44 \qquad (W) \tag{2-6}$$

Power in total length:

$$P = (\varphi \cdot \frac{l}{A}) \cdot I^2 = 0.89 \qquad (W) \tag{2-7}$$

Therefore, the rate at which energy is generated by a passing current through a medium with an electrical resistance known also as body heat flux is calculated. The final answer was

calculated using millimeters due to the complexity of simulating minute dimensions such as the diameter of copper wire. Total Body Heat Flux:

$$\dot{\Delta} = \frac{P}{V} = \frac{\rho \cdot I^2}{A^2} = 7.96e^7 \quad \left(\frac{W}{m^3}\right) \tag{2-8}$$

$$7.96e^4 \qquad \left(\frac{W}{mm^3}\right)$$

2.2 Heat Dissipation

As discussed before, electrical components are ubicated in an enclosure, that tends to be smaller each time. For this reason, accumulation of heat rises; which can potentially damage the electrical and electronic devices. All electronics produce excess heat and overheating can shorten life expectancy and lead to premature failure.

2.2.1 Convection

There are three mechanisms in which energy in form of can be transferred:

- Conduction
- Radiation
- Convection

To dissipate heat, convection is considered, which is defined as "*The mechanism of heat transfer through a fluid in the presence of bulk fluid motion."* [24]. Conduction and convection are similar mechanism since both requires the presence of a material medium. Yet, the difference is that convection requires the presence of fluid motion. Heat transfer through a solid is referred always by conduction, however, heat transfer through a fluid can be done by conduction or convection. When it is through a fluid in this case (air), it enhances heat transfer since it brings

hotter and cooler masses of fluid into contact, giving thus greater rates of heat transferred. The rate of heat transfer increases as the velocity of the fluid increases since this is a strong function of velocity [24]. Convection can be classified as natural or free convection and forced convection.

2.2.2 Natural Convection

Typically, airflow is either classified as natural or forced convection. In forced convection, the fluid is forced to move by an external medium such as fan or a pump. Natural convection is a condition with no external induced flow and heat transfer depends on the air surrounding the electrical component. Fluid velocities in natural convection are low, often less than 1 m/s. Thus, heat transfer coefficients are lower than those in forced convection. However, the intent to dissipate heat through natural convection was because 3D printed components with integrated circuits are manufactured without the need to assemble more components. Forced convection would be more effective to cool electronics; however, a fluid mover would be required. Nonetheless, the objective of printing electrical components in a single step without assembling would be lost.

2.2.3 Heat Transfer Coefficient

To calculate the heat transfer coefficient on polycarbonate, there are several steps that are need it to be followed. Forced convection is governed by the dimensionless Reynolds number. On the other hand, natural convection is governed by the Grashof number; which is a dimensionless parameter that represents the natural convection effects [25]. In other words, it represents the correlation of heat and mass transfer due to thermally induced natural convection at a solid surfaced immersed in a fluid. It is defined as:

$$Gr_L = \frac{g \cdot \beta \cdot (T_S - T_\infty) \cdot {L_c}^3}{\vartheta^2} \tag{2-9}$$

Where:

g = gravitational acceleration (m/s^2)

β = coefficient of volume expansion, (1/K)

T_s = temperature of the surface, (℃)

T_∞= temperature of the fluid sufficiently far from the surface, (℃)

L_c = characteristic length of the geometry, (m)

ϑ = kinematic viscosity of the fluid, (m^2/s)

Properties of the fluid (air) necessary to calculate the heat transfer coefficient where taken from Table A.4, Heat and Mass Transfer Fundamentals and Applications book; at a film temperature of 338 kelvins. As shown in Table 2.3 below:

Table 2.3: Properties of air at a film temperature of 338 Kelvins

Film Temperature (T_f) K	Thermal Conductivity (κ) $W/(m \cdot k)$	Thermal Diffusivity (α) $m\text{^}2/s$	Kinematic Viscosity (ν) $m\text{^}2/s$	Prandtl Number (P_r)	Volume Expansion (β) $1/K$
338	0.028445	$2.706e^{-5}$	$1.9455e^{-5}$	0.7177	220

Natural convection on a surface depends on the geometry, orientation, thermo-physical properties of the fluid, among other factors. To calculate heat transfer coefficient, a well-known correlation for the average number Nusselt Number (Nu) in natural convection has the form of:

$$\overline{Nu}_L = \frac{\overline{h \cdot L}}{k} = C \cdot (Gr_L \cdot \mathrm{Pr})^n = C \cdot {Ra_L}^n \tag{2-10}$$

Where Rayleigh number is the product of Grashof and the Prandtl number obtained with the film temperature of the fluid (air). With properties of air at film temperature of 338 kelvins the Rayleigh number is calculated

$$Ra_L = Gr_L \cdot Pr = \frac{g \cdot \beta \cdot (T_s - T_\infty) \cdot {L_c}^3}{\vartheta \cdot \alpha} \tag{2-11}$$

$$Ra_L = Gr_L \cdot Pr = \frac{9.81 \cdot 0.00295 \cdot (100-30) \cdot {L_c}^3}{1.8455e^{-5} \cdot 2.706e^{-5}} = 3.84e^9 \cdot L^3 = \ 4.49e^4$$

As shown above, the free convection boundary layer is laminar. Therefore, the equation used for the Nusselt number used is the following; since the equation accounts for small Rayleigh number ($10^4 \leq Ra_L \leq 10^9$). After calculating the Nusselt number, equation (2-10) is solve for the heat transfer coefficient giving, $10.24\frac{W}{m^2 \cdot k}$

$$\overline{Nu_L} = 0.68 + \frac{0.670 \cdot {Ra_L}^{1/4}}{\left[1+(0.492/Pr)^{9/16}\right]^{4/9}} \tag{2-12}$$

$$\overline{Nu_L} = 0.68 + \frac{(0.670 \cdot 4.49e^4)^{1/4}}{\left[1+(0.492/0.7177)^{9/16}\right]^{4/9}} = 8.173$$

$$h = \frac{k}{L} \cdot \overline{Nu_L} = 10.24\frac{W}{m^2 \cdot k}$$

$$\boxed{10.24\frac{W}{m^2 \cdot k}}$$

2.3 Validation

2.3.1 Maximum Temperature in Cylindrical Coordinates

In this section, the maximum temperature in cylindrical coordinates with inner radius power is calculated. Dimensions of the cylinder are shown in Figure 2.2. The main goal is to validate the data obtained in FEA simulation explained in chapter 3, and to assure that the electronic device is corrected modeled in the FEA analysis. In many situations, heat conduction can be approximated as being one-dimensional, since heat is expected to be dominant in one direction and negligible in other directions.

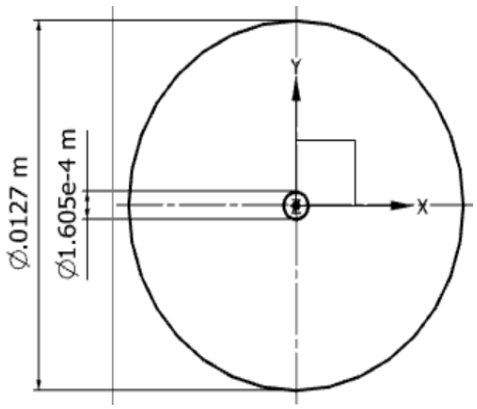

Figure 2.2: Dimensions of Polycarbonate cylinder with embedded copper wire

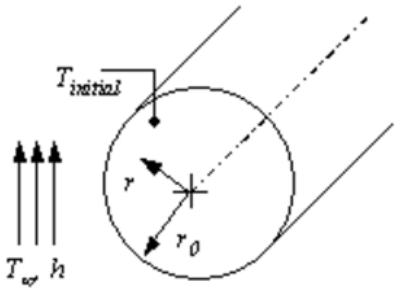

Figure 2.3: Boundary Conditions

Heat conduction in cylindrical coordinates follows the general differential equation:

$$\frac{\partial^2 T}{\partial r^2} + \frac{1}{r}\frac{\partial T}{\partial r} + \frac{1}{r^2}\frac{\partial^2 T}{\partial \phi^2} + \frac{\partial^2 T}{\partial z^2} \tag{2-13}$$

To get maximum temperature, the assumption of a 1-Dimensional Steady State problem was made, simplifying the general differential equation to:

$$\frac{1}{r}\frac{\partial T}{\partial r} + \frac{\partial^2 T}{\partial r^2} = 0 \tag{2-14}$$

With the following Boundary Conditions displayed in Figure 2.3: equation (12-15) determines the rate of heat transfer and thus the heat flux q (heat transfer rate per unit surface area W/m^2); this information is used as the first boundary condition. Where the heat flux can be expressed by Fourier's law of heat conduction as:

$$\frac{\partial T}{\partial r}\bigg| r_i = -\frac{\dot{q}_w}{k} \tag{12-15}$$

Where:

$$q_w = \frac{\dot{s}}{2 \cdot \pi \cdot r_i} \tag{12-16}$$

Convection was used as a second boundary condition. This is because, heat transfer cylinder surface is expose to the environment at a specific temperature. The convection boundary condition is based on a surface energy balance expressed as:

$$(k\frac{\partial T}{\partial r} + hT)|r_o = h \cdot T_\infty \tag{12-18}$$

Double integration will give:

$$T(r) = C_1 + C_2 \cdot \ln(r) \tag{12-19}$$

Using boundary conditions 12-15 and 12-16 gives:

$$T(r) = \frac{\dot{s}}{2\cdot\pi} \cdot [\frac{1}{h\cdot r_o} + \frac{1}{k} \cdot \ln(\frac{r_o}{r})] + T_\infty \tag{12-20}$$

Properties of polycarbonate [32] are necessary to calculate maximum temperature where are shown below (see Table 2.4):

Table 2.4: Thermal properties of Polycarbonate

Polymer	Density $(\boldsymbol{\rho})$ $\boldsymbol{Kg/m^3}$	Thermal Conductivity $(\boldsymbol{\kappa})$ $\boldsymbol{W/(m \cdot k)}$	Thermal Expansion $(\boldsymbol{\alpha})$ $\boldsymbol{K^{-1}}$	Specific Heat $(\boldsymbol{cp})$ $\boldsymbol{J/K \cdot Kg}$
Polycarbonate	1430	0.022	$70e^{-6}$	1200

To calculate maximum temperature $T_{max} = T(r_i)$, temperature at the inner radius is calculated with equation 2.18 using thermal conductivity of polycarbonate and the heat transfer coefficient calculated in section 2.2.3.

$$T_{max} = \frac{\dot{s}}{2\cdot\pi} \cdot [\frac{1}{h\cdot r_o} + \frac{1}{k} \cdot \ln(\frac{r_o}{r_i})] + T_\infty \tag{2-21}$$

Where $\dot{s}$ refers to the joule heating per unit length. Current was the same used to calculate body heat flux, 5.5 amperes and the resistivity of copper wire.

$$\dot{s} = \frac{I^2 \cdot \varphi}{\pi \cdot {r_i}^2} \tag{2-22}$$

$$\dot{s} = \frac{5.5^2 \cdot 1.724e^{-8}}{\pi \cdot (1.605e^{-4})^2} = 6.4$$

Giving an expected maximum temperature of:

$$T(r_{max}) = \frac{6.44}{2 \cdot \pi} \cdot \left[\frac{1}{10.24 \cdot 0.127} + \frac{1}{0.22} \cdot \ln\left(\frac{0.0127}{(1.605e^{-4}}\right)\right] + 30$$

$$T_{max}(r) = 58.24\ ℃$$

3. Finite Element Method

3.1 Overview

This chapter will discuss in detail the thermal analysis performed on the Polycarbonate block with an embedded copper wire acting as joule heating by finite element (FE) methods. As mentioned before, this section attempts to explain and provide the process followed to simulate the predicted maximum temperature and heat dissipation in the polymer with joule heating through natural convection. The main objective of a detailed FE analysis is to predict and modify to enhance, heat dissipation. Thus, FEA produces a more detailed set of results and information compared to experimental procedures *i.e.* 3D manufacturing. Moreover, it is often faster and less expensive than experimental procedures. Some of the advantages of (FE) analysis are:

- Create physical or thermal responses at any location including some that might be neglected in an analytical approach.
- Anticipate failure of the model without risk.
- Clear visual representation of parameters (Temperature and Heat Fluxes), allowing a better analysis and faster modifications if needed.
- Relatively low investment and faster calculation time compare to experimental procedures.
- FE analysis allows to test the performance of the component, once obtained the desirable results it can be manufactured.

The thermal analysis of natural convection in 3D printed electronics was done in the finite element analysis software Abaqus 6.14 [33]. Additional auxiliary software where used to sketch and mesh the geometry (NX 8.5) and (Hypermesh 13.0).

3.2 FEA set up for base model

3.2.1 Model Description

The first thermal simulation was performed on the original polycarbonate block with and embedded wire with joule heating running along the polymer. The following picture shows the 3D printed polycarbonate with copper wire printed at the W.M. Keck Center for 3D innovation laboratory located at The University of Texas at El Paso.

Figure 3.1: 3-D Printed Polycarbonate block with embedded copper wire printed at the W.M. Keck Center

As mentioned in chapter 2, section 2.1.3, a body heat flux was applied to simulate the joule heating effect that copper wire will produce. The heat transfer coefficient will be applied to the faces of the polycarbonate block that are in contact with the fluid (air). The parameters mentioned before will be explained further in the FEA model set up.

3.2.2 Geometry

As mentioned in section 3.1, geometry was sketched in the computer-aided software (N.X 8.5). This is because, NX provides advance geometry capabilities, making easier to sketch, modify complex models. Otherwise would be difficult using a software with deficient sketching capabilities. The base model was sketched in millimeters due to the complexity of modeling very small diameters and overall dimensions *i.e.* copper wire. The model was sketched using the

symmetrical quarter portion of the geometry. This will give a simplified model without altering the predicted results. The dimensions for the full portion of the polycarbonate block and the copper wire are shown in Table 3.1

Table 3.1: Base model dimensions

Component	Length (L) **mm**	Height (H) **mm**	Width (W) **mm**	Diameter ($\emptyset$) **mm**
Polycarbonate	138.1	22.7	30.2	n/a
Copper Wire	140	n/a	n/a	0.321

Below, two sketches are shown where: Figure 3.2 displays the full sketch of the polycarbonate block (gray) with embedded wire (yellow) and Figure 3.3 shows a quarter portion of the model; the quarter will be used for mesh and simulation. After the sketching in NX 8.5 was finalized, the geometries were exported as two separate IGES files.

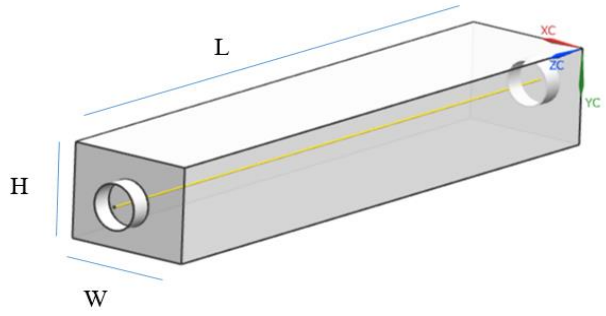

Figure 3.2: Full sketch of the polycarbonate block

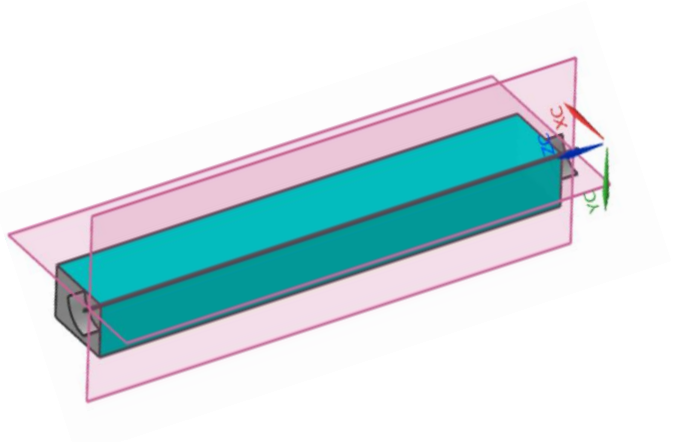

Figure 3.3: Quarter portion of the model

3.2.3 Mesh

Both IGES files were exported as two different components to Hypermesh 13.0; which is a finite element pre-processor with potent capabilities to mesh complex geometries in automatic or semi-automatic mode. Hypermesh was chosen to mesh the 3D printed electrical device since

this software allows manual control over the quality of the mesh, compare to other software with restricted control over the mesh. The mesh of the base model, was done in two parts. The quarter of the polymer block is a simple geometry; therefore, 2D finite elements were used to create a high-quality mesh. 2D elements are used when two of the dimensions are small in comparison to the third one [34]. In this case, the length of the polymer and the copper wire are large compare to the height, width and diameter respectively. Quadrilateral elements where used for the mesh, instead of tria elements due to the simplicity of the figure.

Two main factors where considered to increase the quality of the mesh. The first factor considered was the effect of mesh density. In other words, the density or number of elements was increased in the area where the wire is embedded; this is because, temperature and heat fluxes are expected to have a higher impact in this area (also called critical region), due to the proximity to the heat source. The second factor considered was the effect of biasing the critical region. In other words, bias increases the concentration of elements at certain region (critical region) to obtain accurate results. Figure 3.4 shows a close view of the factors considered, density and bias were increased at critical region

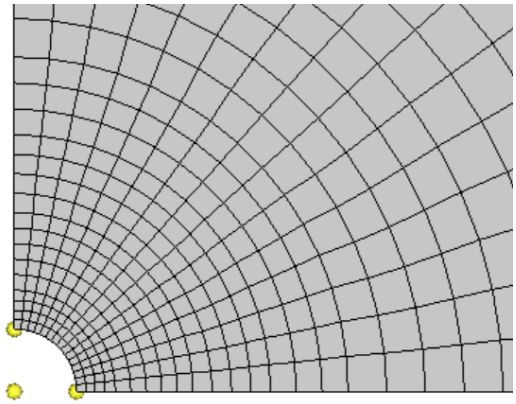

Figure 3.4: Close view of the increased mesh density and bias at critical region

After creating a high-quality mesh with 2D elements, the elements where drag to create a 3D element component. Same process was performed for the copper wire, and both meshes where

exported as two different input files to start thermal simulation. Figure 3.5 displays the final mesh for the base model.

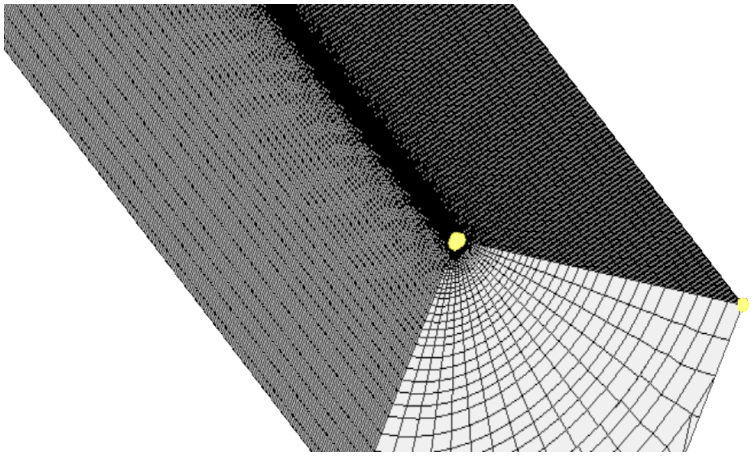

Figure 3.5: 3-D mesh created through 2-D mesh projection

3.2.4 Simulation

As mentioned before, Abaqus 6.14 was used to perform the (FE) thermal analysis on the polycarbonate with embedded copper wire using standard/explicit model. The thermal analysis will model and solve for temperature distribution and maximum temperature within the polycarbonate block at steady state conditions and the heat flux across the block. To do this, the meshes created in Hypermesh were exported as input files to Abaqus; this created orphan meshes, which means that there is no geometry in the model. The elements in the mesh were change from 3D stress elements to DC3D4: 4 node linear heat transfer tetrahedron to perform a thermal analysis. Also, two material properties where define including polycarbonate and copper. As discussed previously, the geometry was sketched in millimeters as dimensions are too small to sketched in meters. For this reason, all properties where converted to millimeters, including: density, thermal expansion, thermal conductivity and specific heat. After that, two sections were created to assign the material to each component. Then, a step was created with steady state heat transfer as the type of procedure. For boundary conditions, one interaction and a load were applied to the model, heat transfer coefficient and body heat flux. First, an interaction is a step dependent object, in this case

in will be analyze in the heat transfer step. The interaction created will be a film condition on the surfaces exposed to the fluid (air) in the polycarbonate. was created to define thermal film conditions. Film condition defines convection from model surfaces and concentrated film conditions from nodes. As calculated in chapter 2, $10.24(\frac{W}{mm^2 \cdot k})$ was used as the film coefficient or heat transfer coefficient and 298 kelvins as the sink temperature. To simulate thermal expansion a load must be applied. Calculated in chapter 2 as well body heat flux of $7.96e^4 \left(\frac{W}{mm^3}\right)$ was used to predict heat dissipation and analyze the joule heating effect. Figure 3.6 shows the two boundary conditions applied to the model.

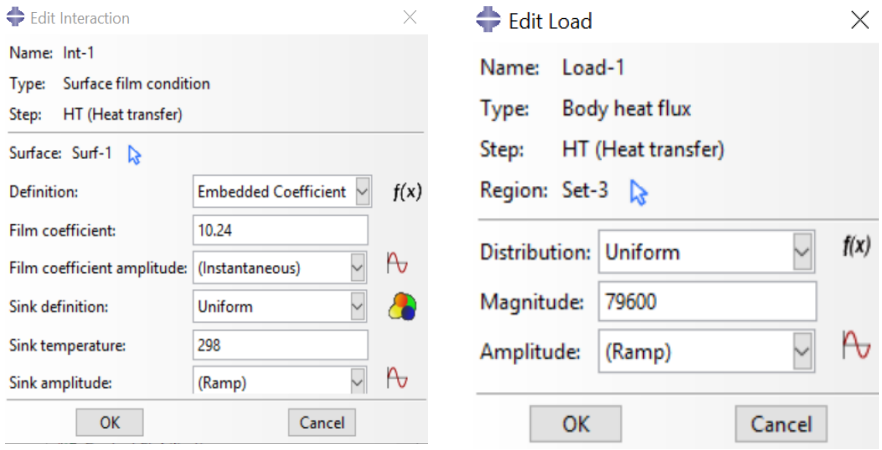

Figure 3.6: Boundary conditions applied to the model

3.2.5 Results

After the FEA analysis was run in Abaqus the results were analyzed. Results for the simulation in the base model showed a maximum temperature of 62.65 ℃ and all heat dissipated through the polycarbonate block. Even though, the temperature is below the glass transition temperature of 100 ℃ it is important to analyze if the component is within safe operating temperatures. An operating temperature is known as the temperature range at which an electrical device operates to remain safe. The device should operate within a specified temperature range which varies based on the device function, application among others. If the device operates above or below those temperatures, premature failure may occur. The ranges include a minimum and

maximum temperature. For a commercial component, the safe operating temperatures ranges from 0 to 70 ℃ [35]. For this reason, base model increases the temperature of the polycarbonate considerably, which results in the deformation and decrease in the reliability of the material. Figure 3.7 shows maximum (red) through minimum temperature (blue) expressed in kelvins at nodes (NT). Maximum NT11 shows 62.65 ℃. In section 2.3., the maximum temperature in cylindrical coordinates with inner radius power was calculated. The objective was to validate the FEA simulation trough mathematical calculations. As previously discussed, the maximum temperature in the mathematical calculation was 58.24 ℃ giving a low error of 6.83% that validates the reliability of the FE thermal analysis.

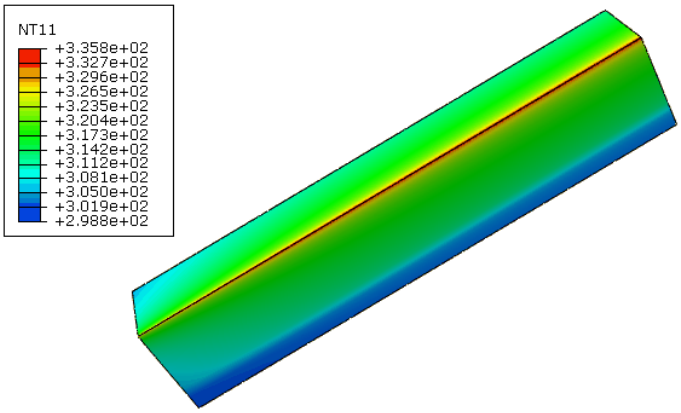

Figure 3.7: Base model temperature profile

3.3 Proposed Designs

To improve and dissipate the heat generated by the heating wire and lower the overall temperature, three designs were proposed. The main goal is to ease heat dissipation by adding additional "auxiliary" wires with no current. The first and second proposed designs consisted in:

- Polycarbonate cylinder
- Embedded radial array of six auxiliary copper wires for the first design (See Figure 3.8)
- Embedded radial array of eight auxiliary wires for the second design.

In addition, the second design has radial fins to create a radial heat sink. The objective of the second design was to carry heat into the fins that provide a large surface are for the heat to dissipate through natural convection as observe in Figure 3.9. On the other hand, the third design consisted in a polycarbonate block with additional wires running along the heating source and going out of the polycarbonate at every determined distance as shown in Figure and 3.10. Similarly to the second design, the polycarbonate block has rectangular fins that carry the thermal energy out into the surrounding air. Figures 3.8-3.10 show the thermal analysis performed on the three proposed designs to improve heat dissipation and to lower temperature. Moreover, it is important to mention that each design were analyzed using symmetry. In other words, only the quarter portion of the whole model was simulated for a simplified model without altering the results. However, these designs were not taken into further consideration for an optimization for the following reasons:

- Thermal Finite Element Analysis performed in Abaqus showed minimum heat dissipation through the additional wires, less than 2%
- The overall decrease of temperature in the component was not significant.
- More independent variables would have to be taken into consideration to optimize the response. This will be explained in detail in Chapter 4.

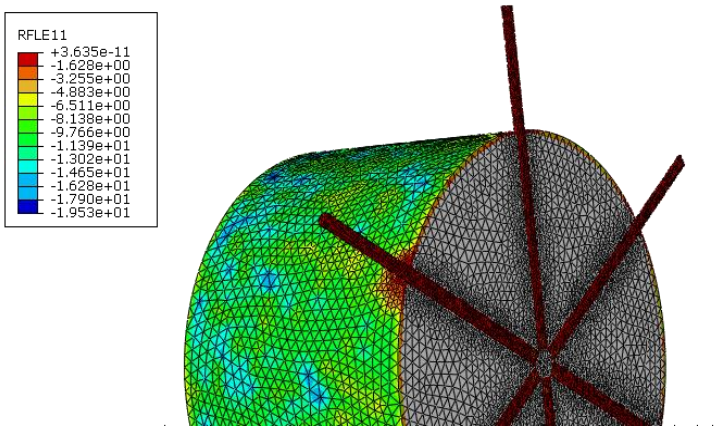

Figure 3.8: First proposed design with six radial embedded wires

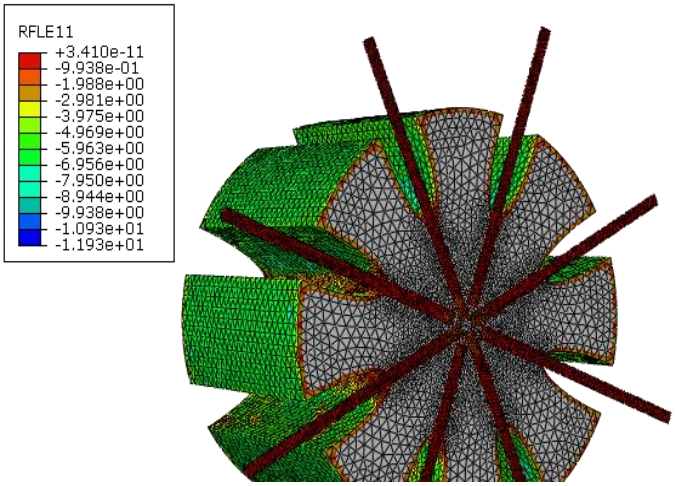

Figure 3.9: Second proposed design with eight radial embedded wires

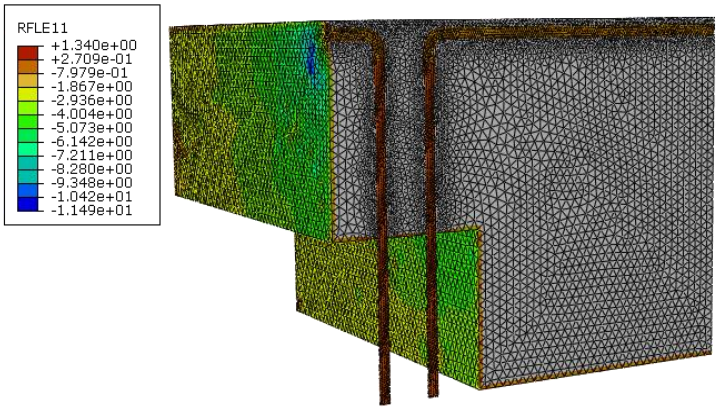

Figure 3.10: Third proposed design with wires running along the heating source

3.4 FEA set up for model with deposited metal

3.4.1 Model Description

This section fully explains the intent to develop a fourth proposed design that will ease heat dissipation through deposited metal wires with not current as mentioned in section 3.4. The deposited metal will be additional to the joule heating wire. As explained in previous section, base

design manufactured at the W.M Keck center for 3D innovation laboratory, rises the temperature of the overall component at unsafe operating temperature. Therefore, the importance of creating a new component design that will lower the temperature and increase heat dissipation. New design consists in:

- Deposited copper wires without current. In addition to the copper deposited in the FDM process for the circuitry, additional metal is deposited to help conduct the heat generated by the joule effect.
- Decrease the overall size of polycarbonate.

Furthermore, this design aims to decrease temperature in the 3D printed polycarbonate component; by facilitating the dissipation of heat generated by the joule heating wire through the additional deposited copper wires. To achieve this, copper was chosen as the material for the additional wires, due to the high thermal conductivity of the material compare to polycarbonate. Thus, it will facilitate heat dissipation through the wires instead of the polycarbonate. Further section will explain the geometry, mesh and set up to perform a FE thermal analysis.

3.4.2 Geometry

Using similar base model procedure, the new design was sketched in the computer-aided software (N.X 8.5) and was also sketched in millimeters. The model was also sketched using the symmetrical quarter portion of the geometry. This will give a simplified model without altering the predicted results. The dimensions for the full portion of the polycarbonate block and the copper wire with the additional copper wire are shown in Table 3.2

Table 3.2: New Design dimensions (Full Portion)

Component	Length (L) **mm**	Height (H) **mm**	Width (W) **mm**	Diameter ($\emptyset$) **mm**
Polycarbonate	101.6	2.54	50.8	n/a
Copper Wire	103	n/a	n/a	0.321

Figure 3.8 displays half of the model sketched in NX 8.5; to the right, the quarter of the whole design is displayed for a clearer understating of the portion that will be simulated. It is important to clarify that deposited metal will behave as a pattern along the total length of the geometry. (Gray) component represents the polycarbonate; then, (orange) component characterizes the joule heating wire and finally (yellow) component represents the additional deposited metal. After the sketching in NX 8.5 was finalized, the geometries were exported as three separate IGES files.

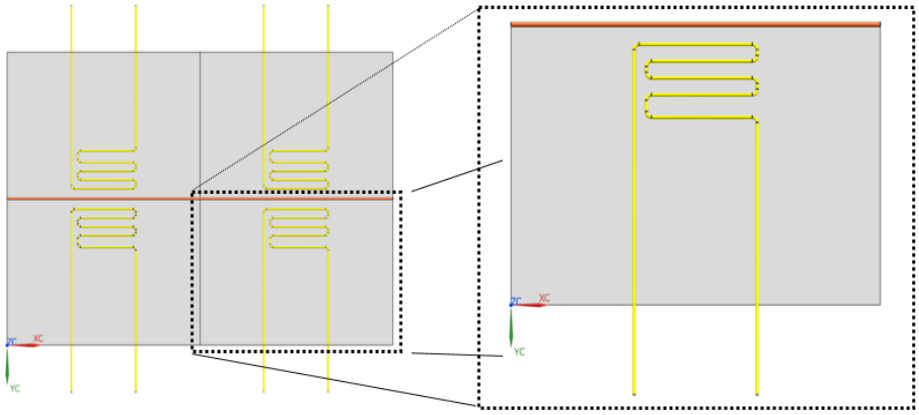

Figure 3.11: Half representation of the model (Left), Quarter representation of the model (Right)

3.4.3 Mesh

The three IGES files were exported as three different components to Hypermesh 13.0. As mentioned before, the symmetrical portion of the model sketched, this will help to increase the

density of the mesh to achieve a greater accuracy and still have fewer elements than if the entire model was analyzed. This design has a more complex geometry; thus, 3D elements where used instead of 2D elements used in base model. There are several meshing techniques offered in Hypermesh to create 3D elements. The technique applied for this design was 2D (tria) to 3D (tetra). Quad or tria meshing was carried out separately for each component. During this process, quad elements are automatically split into trias, which serves as the basis of the tetra elements. After creating the mesh, (see Figure 3.9) the size of the element was change to have a maximum element size of 0.3 and minimum element size of 0.2. Moreover, in the new model there are small areas of curvature *i.e*. copper wires. Consequently, curvature and proximity option was applied to the mesh to refine elements in these areas (see Figure 3.10).

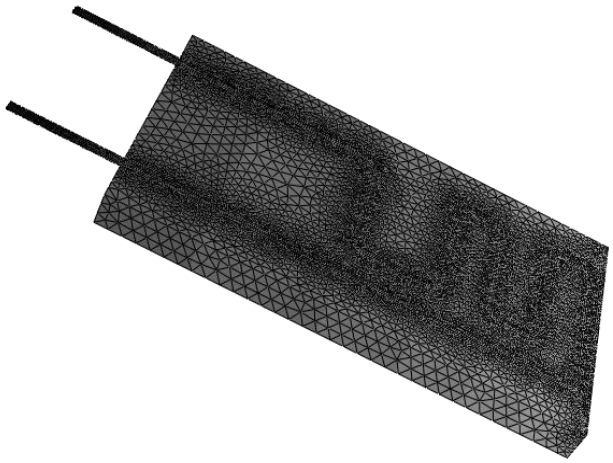

Figure 3.12: Geometry meshed with 3-D Elements

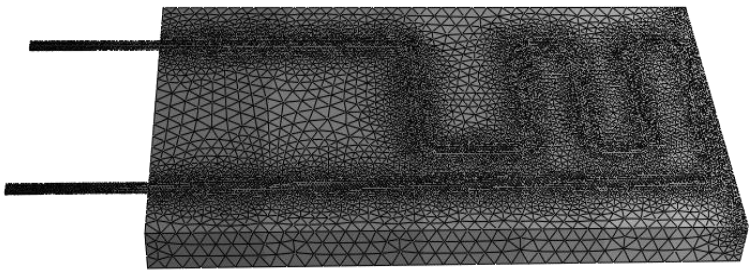

Figure 3.13: 3-D Mesh using curvature and proximity

Once every component was meshed with same size elements, it was essential to equivalence the elements. In other words, since geometries were mesh in different parts, it is important to check any disconnected elements by equivalent the elements in 'tool panel' in Hypermesh. This will ensure that the three meshes are connected for a high-quality and reliable simulation of heat dissipation and temperature (see Figure 3.11). Lastly, the quality of the mesh was checked by testing the tet collapse. In other words, if tetra elements whose collapse values fall below the value specified are highlighted. The meshes created where tested using 0.3 as the tet collapse value. The number of failed elements were 0 of the 608363 elements created, an acceptable number is approximately 120; therefore, the quality of the mesh is high. Figures 3.9 and 3.10 show the meshes of each component of the new circuitry design.

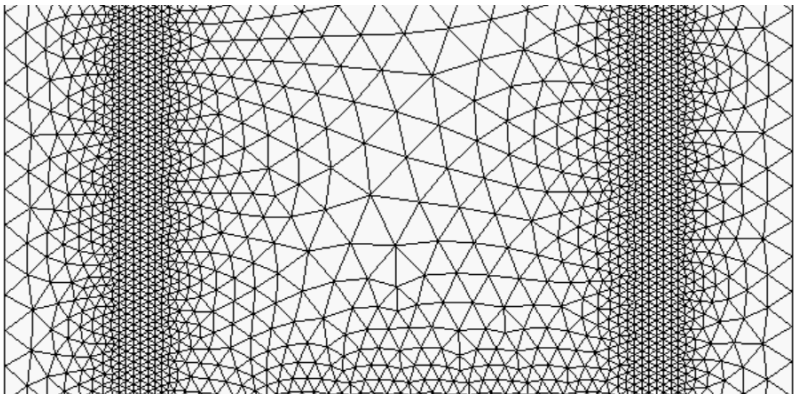

Figure 3.14: Connected mesh by using equivalence in Hypermesh

3.4.4 Simulation

Even though, the set up to perform a FE thermal analysis in Abaqus 6.14 is comparable to the base model analysis; additional procedures were followed to simulate heat dissipation and temperature distribution. Comparatively to base model simulation, this thermal analysis simulation models and solves as an output variables for temperature distribution and heat flux across the circuitry. Nevertheless, an additional output variable was requested; total flux at nodes, including flux convected through the node in convection elements and excluding external flux such as film

conditions and concentrated fluxes is simulated. This variable output is essential for further calculations explained later in the section.

First, meshes created in Hypermesh were exported in three different input files to Abaqus. This gave three orphan meshes without geometry; consequently, elements where change to DC3D4 which accounts for 3D elements in solids for heat transfer analysis in Abaqus. As discussed before, two material properties copper and polycarbonate were defined in Abaqus for base model; likewise, for the second design simulation. Properties needed to calculate thermal dissipation and temperature are, density, thermal expansion, thermal conductivity and specific heat for both, copper and polycarbonate. After three sections were created to assign the material for each component, two additional sets where created. The first set included the additional deposited wires and the second set included only the surfaces in contact with air (convection). Then, a step was created with steady state heat transfer as the type of procedure. For boundary conditions, two interactions and a load were applied to the model, heat transfer coefficients and body heat flux. To emphasize, an interaction is a step dependent object, in this case in will be analyze in the heat transfer step. The interaction created was a film condition on the surfaces exposed to the fluid (air) in the polycarbonate. In addition to the first interaction, a second film condition was created on the deposited copper wires to define thermal film conditions. Film condition define convection from model surfaces and concentrated film conditions from nodes. As calculated in chapter 2, $10.24(\frac{W}{mm^2 \cdot k})$ was used as the film coefficient or heat transfer coefficient and 298 kelvins as the sink temperature for both interactions created. To simulate thermal expansion a load must be applied. Same body heat flux of $7.96e^4 \left(\frac{W}{mm^3}\right)$ was applied to the joule heating wire to predict heat dissipation. After that, two additional field output were requested. The first one requesting thermal variable outputs for the wires set previously created, and the second requesting thermal variables outputs as well, but for the set of surfaces in contact with air. As final step, a job was created to be analyzed. Figures 3.12 and 3.13 show both interactions and the load applied to the components.

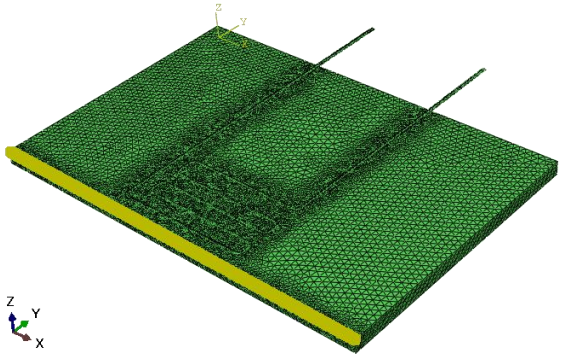

Figure 3.15: Body heat flux load

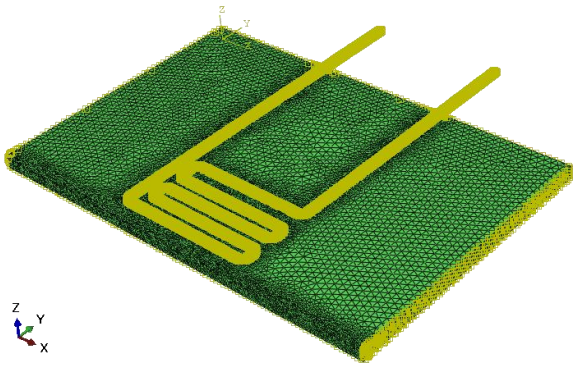

Figure 3.16: Surface Film Condition Interactions

3.4.5 Results

Results for the simulation in the new model design showed an undesirable output. As a matter of fact, the simulation showed a maximum temperature of 118.05 ℃. This design, increased temperature considerably compare to base design simulation. After the simulation was completed an additional procedure was done to calculate the total heat flux out the deposited wires and the polycarbonate surface. After the simulation was ran, an *.inp file (input file) is automatically created. This is a text file that Abaqus solver reads, and it is possible to manually create it or modify and request output. In this case, the input file was modified to request the total heat flux out from the deposited copper wires and the polycarbonate surfaces. As explained before, sets were created to modify the input file. The following lines are added to the input file and saved:

*Node Print, nset=”Set-Wires”, totals=yes

RFLE11

*Node Print, nset=”Set-Square”, totals=yes

RFLE11

Once it is saved, the input file is run once again in Abaqus command window by calling the job:

Abaqus job=Job name

Old job files exist. Overwrite? (y/n)

This command will run the model once again to get the heat flux of the specified nodes; as well as the sum of the total heat flux out of the created node sets. This information will be created in *.dat file. As observed in Figure 3.14, RFLE11 represents the total flux out convected through the node in convection elements. In other words, it is the total heat flux out by convection surfaces. Heat flux is referred as the rate of heat energy transfer through a give surface per unit time [24]. Negative sign shows that heat flux is moving from a high temperature to lower regions. Low values of RFLE11, demonstrate that most of the heat flux is getting out through these surfaces. In other words, Figure 3.14 demonstrates that most of the heat is being dissipated from the lower part of the polycarbonate; which, is the area closer to the joule heating wire.

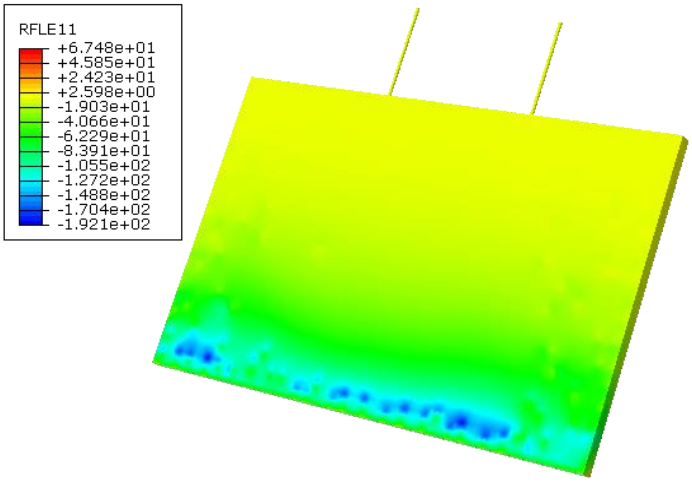

Figure 3.17: Total Heat Flux out (Polycarbonate)

On the other hand, Figure 3.15 shows another angle of the model showing the deposited copper wires; which objective is to dissipate heat. This figure clearly demonstrates that heat flux out through the deposited copper wires is relatively low. As a matter of fact, after analyzing the *.dat file, it was calculated that only 9.49% is dissipated through the wires and 90.51% is dissipated through polycarbonate.

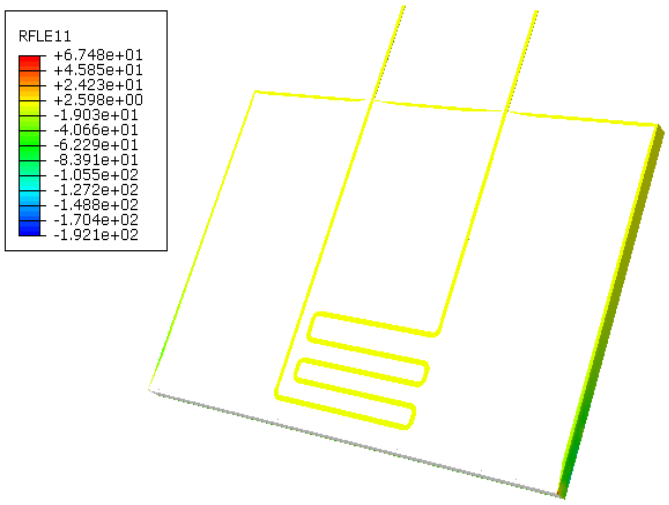

Figure 3.18: Total Heat flux out (Deposited copper wire)

Moreover, as explained before, the temperature is not within safe operating temperature; not to mention that, temperature is above the glass transition temperature of polycarbonate. However, a portion of the heat generated by the joule heating wire is being dissipated through the deposited copper wires. Considering these undesirable results, chapter 4 will discuss in detail the optimization process to achieve a lower temperature and higher dissipation through the deposited wires by following a parametric optimization. To accomplish this, more than 50 computational FEA thermal simulations were made to obtain an optimal design that lowers the overall temperature of the component and increase heat dissipation through the auxiliary wires. Figure 3.16 displays temperature profile NT of the simulation showing 391.2 kelvins as the higher temperature.

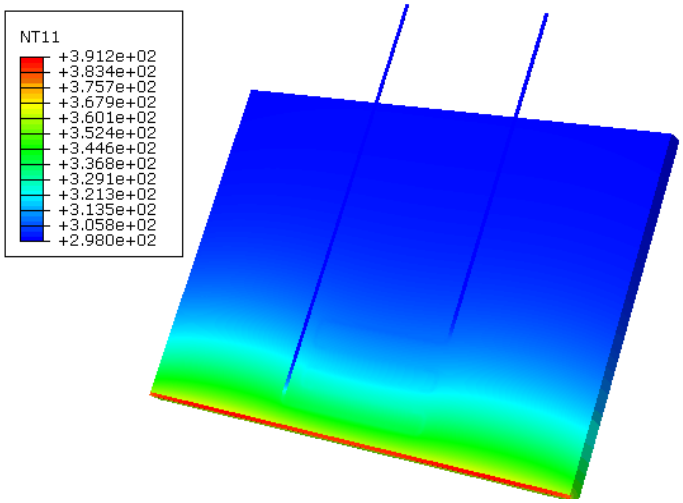

Figure 3.19: Temperature Profile (NT11)

4. Optimization by Response Surface Methodology

4.1 Overview

This chapter will discuss and fully explain the process followed for a parametric optimization. The word optimization, refers to improving the performance of a system, process or a product, in order to obtain the maximum benefit from it [40]. Hence, parametric optimization aims to supply valuable information to find the relevance in variables and to identify possible optimization potentials [36]. In other words, a parametric analysis provides guided methods to achieve an ideal design. Based on the existing finite element model developed; a parametric study is applied to provide sufficient information that enables the optimization of the FE model. Therefore, an improve in the responses (temperature and heat dissipation).

Traditionally, optimization was carried out considering the influence of one factor at a time on a response. This means, that only one variable is change while others are kept fixed. This optimization technique has several disadvantages such as: it does not include the interactive effects among variables (factors) studied and an increase in the number of simulations to find an optimal result [41]. For this reason, optimization procedures have been carried out using multivariable statistics techniques. One of the most used multivariable techniques is Response Surface Methodology (RSM). Explain more in detail, response surface methodology (RSM) consists of a group of mathematical and statistical techniques used in the development of an adequate functional relationship between a response of interest, (Y), and a number of associated control (or input) variables denoted by (x1, x2,…,xk) [37]. Therefore, (RSM) was chosen to help determine the optimum design that will maximize heat dissipation through deposited wires and minimize the temperature of the component having multiple variables (dimensions). Section 4.2 will explain the employed statistical techniques to achieve a design optimization.

4.2 Optimization methodology

Often, it is common to assume that the outcome of an experimental or computational procedure is dependent on the one or multiple variables. In other words, that the result can be describe as a function base on the independent variables.

$$Y = f(x)$$

In any design optimization, it is known that several variables or factors may influence the result. For that reason, a screening design or an experimental plan is performed in order to determine the independent variables and interactions that have significant influence on the result (response). The main goal is to collect data, analyze data and post process the collected data to find a result. To achieve this, first it is important to identify the objective of the simulation as well as the dependent and independent variables.

- Design objective: Increase heat dissipation through deposited copper wires and lower overall temperature of the component

- Define Responses (Dependent variables): For the model, the response of interest (Y) is known to be the dependent variable (heat dissipation and temperature). In other words, this variable changes in response of the independent variable.

- Define input factors (Independent variables): The input variables (x), are defined as independent; that means they can purposely be changed to alter the response. For our design, input variable are the dimensions displayed in the following Figure. The Figure shows the new proposed design for the 3-D printed circuitry, with dimensions (a, b, n, f, h, and w) considered as the input variables. Where (a) represents the total width of the deposited copper wires, (b) shows the distance between one set of wires and the other, (n) is the number of wire passes, (f) represents the distances between the passes, (h) is the height of the component and (w) represents the total width of the polycarbonate.

Once the list of input variables to be analyzed has been completed; an experimental design is chosen to estimate the influence of the different variables on the result. In screening studies, full factorial and fractional factorial designs are common models used. A design of experiments (DOE) is a systematic method used to reunite or collect information that will help find the relationship between input factors and responses. In other words, fractional and full factorial designs of experiments where conducted to find information about cause-and-effect relationships. This was the first approach followed in the optimization process.

After collecting the data from the design of experiments performed an Analysis of Variance (ANOVA) was conducted. ANOVA is used to compare three or more groups of numbers, in this case dimensions will be compare. This analysis is used when several number of runs or experiments are performed *i.e.* design of experiments. An ANOVA test helps to find out if the computational results are significant. In other words, this method will help to figure out if the considered input variables are significant or not [39].

The next step was to perform a regression, which is a method similar to ANOVA. Regression models describe the relationship between a dependent variable, (*Y),* and independent variable or variables, (*X).* Regression are also known as "predictions" since it used the historical relationship between an independent and dependent variable to predict future values of the dependent variable (heat dissipation and temperature) without running simulations. The regression performed was assumed to be linear; and multivariable since more than two input variables were considered. A multiple linear regression model is [38]

$$Y = \beta_0 + \beta_1 \cdot x_1 + \beta_2 \cdot x_2 + \beta_3 \cdot x_3 + \cdots + \beta_i \cdot x_i \qquad i = 1, \cdots, n, \tag{4-1}$$

Where:

- $\boldsymbol{Y}$ Symbolizes the response variable (heat dissipation or temperature)
- $\boldsymbol{\beta_0}$ Represents the y-intercept of the regression line constant term in the model, where β_0 is the constant term in the model.

- $\boldsymbol{\beta_n}$ Represents the slope of the regression line and represent the independent contributions of each independent variable to the prediction of the dependent variable.
- $\boldsymbol{x_i}$ Represents the independent variables (dimensions).

This section explained the methodology employed to optimize the new model. These statistical techniques can be summarized in the following process methodology:

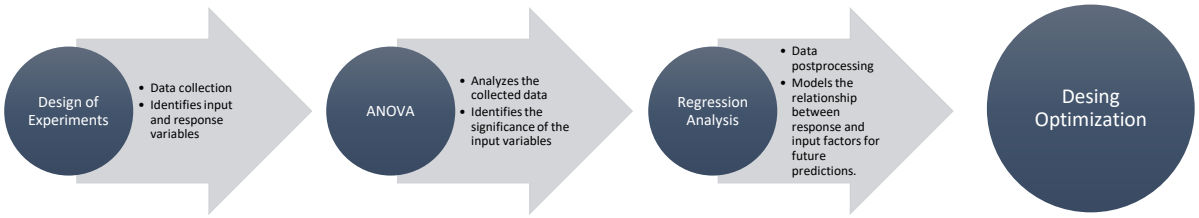

4.3 Model Refinements

4.3.1 First Model Refinement

A factorial design is used to examine the influence of all variables and interaction effects on the responses investigated; as explained before is the process of collecting data. Normally, the input factors are denoted by letter k and can be investigated at two or more levels. A factorial design at two levels is represented as 2^k. Nevertheless, a fractional factorial design was chosen for the first model refinement, since the main goal of this first factorial design is only to identify significance of input variables. The fractional factorial design at two levels is represented as 2^{k-1}. Thus, giving a 2^{4-1} form of fractional factorial design. In other words, k represents four dimension parameters including (**a, b, n**, and **f**) selected as the input factors, displayed in Figure 4.1

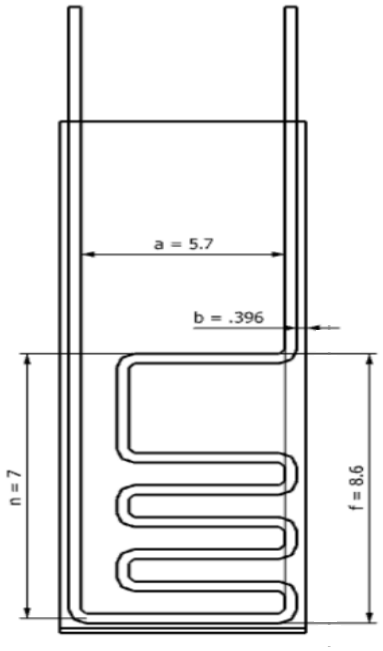

Figure 4.1: Sketch showing input factors considered

In addition, each variable is measured at two levels that are coded as (1) and (2) to represent "low" and "high" values, which will give a total of 8 computational runs. Table 4.1 displays the factors considered for the fractional factorial design with high and low values selected for each variable.

Table 4.1: Input factors evaluated at two levels

Factors	High (1)	Low (2)
a (mm)	9.7	5.7
b (mm)	1.587	0.396
f (mm)	8.6040	6.6040
n (number of passes)	7	5

.

.

Also, Table 4.2 shows in detail eight computational runs performed with all possible combinations coded with (1) and (2) as mentioned earlier.

Table 4.2: Eight computational run combinations

Run Number	Factor (input)			
	a	**b**	**f**	**n**
1	2	2	2	2
2	1	2	2	1
3	2	1	2	1
4	1	1	2	2
5	2	2	1	1
6	1	2	1	2
7	2	1	1	2
8	1	1	1	1

After the eight computational runs were simulated in Abaqus, the obtained results for heat dissipation through deposited wires and temperature where analyze in Minitab. As explained before, ANOVA helps analyzing the obtained data in the design of experiments to find the relevance on each input variable (Data processing). Results of the Analysis of Variance performed in Minitab are shown in Table 4.3. To determine whether the input variables are statistically significant, the P-Values are analyzed. Usually, the significance level (alpha) of 0.05 is an acceptable value. In other words, if P-Values $>$ alpha, represents little or none significance in input variable over the output response. On the other hand, P-values $\leq$ alpha, denotes significance in input variables [42]. Analyzing the P-Values obtained in the first ANOVA, it can be concluded that **a** and **f** do not have a significant impact on the response (*Y)*. On the contrary, **n** and **b** showed high significance.

Table 4.3: ANOVA results for First Model Refinement

Term	Coeff.	SE Coeff.	T-Value	P-Value
Constant	74.29	3.85	19.27	0.003
a	0.436	0.149	2.92	0.100
b	3.911	0.502	7.80	0.016
f	0.195	0.299	0.65	0.581
n	-1.293	0.299	-4.32	0.050

The final process as discussed before, is data postprocessing. In other words, use the data obtained in ANOVA to perform a regression analysis. Explained more in detail, a regression analysis generates an equation that describes a statistical relationship between the analyzed input factors and the response variable. The regression coefficients also shown in ANOVA Table 4.3, represent the mean change in the response variable for one unit of change in the predictor variable while holding other predictors in the model constant [41].

In other words, coefficients can be seen as “slopes” for each input variable. In addition, the regression analysis generates residual plots. First, the normal plot of residuals displays the residuals versus their expected values when the distribution is normal. This plots are used to verify the assumption that the residuals are normally distributed, and should approximately follow a straight line.

Figures 4.2 and 4.3 show normal plot of residuals for heat dissipation and temperature. While Figure 4.2 show that residuals are following a straight line, Figure 4.3, shows discrepancies since the temperature is already low.

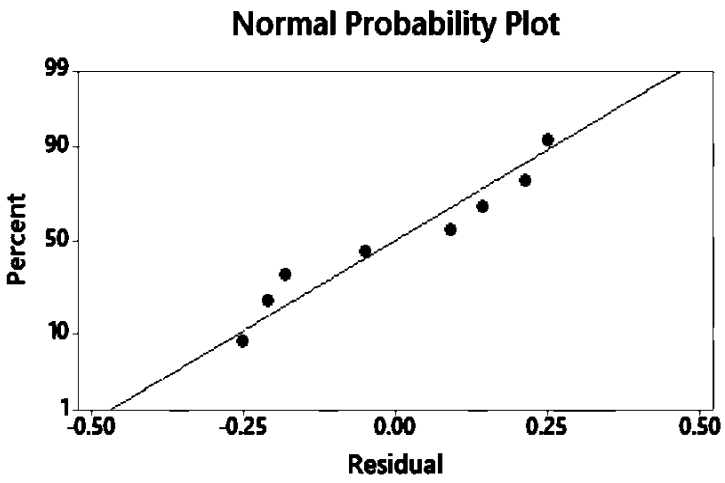

Figure 4.2: Heat dissipation normal probability plot for First Model Refinement

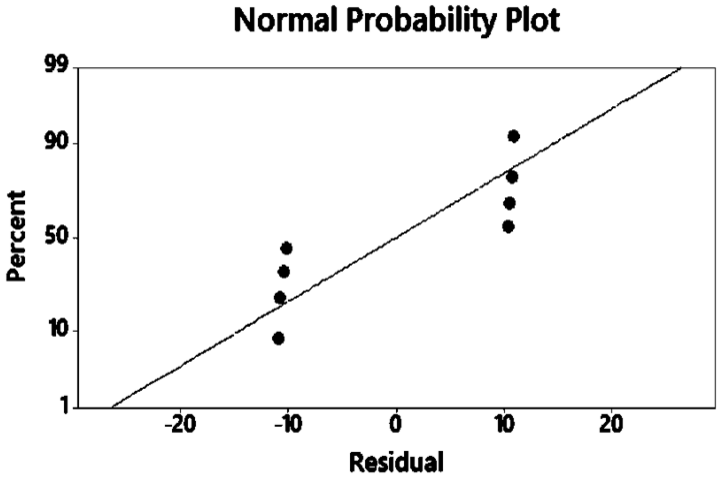

Figure 4.3: Temperature normal probability plot for First Model Refinement

4.3.2 Second Model Refinement

The conclusion after the ANOVA performed in the first model refinement, was that **a** and **f** does not have a significant effect on the response variables. On the other hand, **n** and **b** showed high influence to increase heat dissipation and lower temperature of the component.

For this reason, a full factorial design was considered as the second model refinement with the intent to achieve better responses. A Taguchi L-16 design was considered for the full factorial. This design has the form 4^2 where 2 factors (**n** and **b**) are considered as input variables. Moreover, values of **a** and **f** where fixed, using the values of the best run obtained in the first model refinement. Figure 4.4 shows fixed values of **a** and **f** and factors considered for Taguchi L-16 (**n** and **b**)

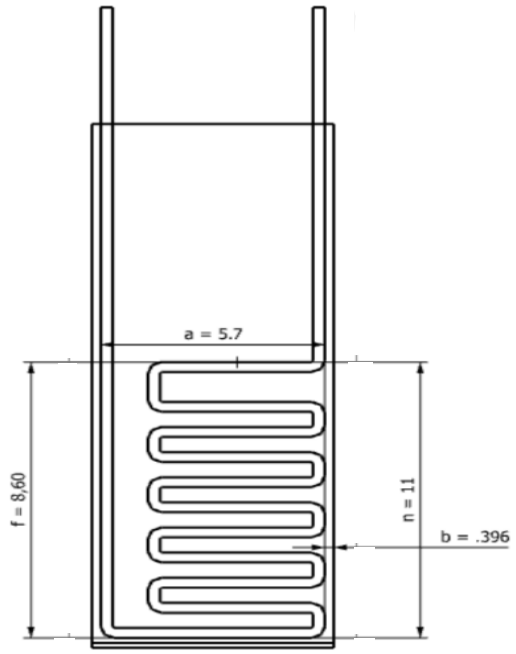

Figure 4.4: Sketch showing input factors n and b with fixed f and a

Also, since this design has the form: 4^2, four levels or values for each factor were selected and coded as (1), (2), (3) and (4); representing, high, medium, standard and low values for each input factor. Table 4.4 displays factors considered as well as the four values at which they will be evaluated.

Table 4.4: Input factors evaluated at four levels.

Factors	High (1)	Medium (2)	Standard (3)	Low (4)
b (mm)	1.65	1.5	0.79375	0.396
n (number of passes)	11	9	7	5

In addition, Table 4.5 shows in detail the 16 computational runs completed with all possible combinations coded with (1), (2), (3) and (4).

Table 4.5: Sixteen computational run combinations

Run Number	Factor (input)	
	n	**b**
1	1	1
2	1	2
3	1	3
4	1	4
5	2	1
6	2	2
7	2	3
8	2	4
9	3	1
10	3	2
11	3	3
12	3	4
13	4	1
14	4	2
15	4	3
16	4	4

Comparatively to the first model refinement, the sixteen results obtained through Abaqus were analyzed in Minitab to perform an Analysis of Variance. Table 4.6 displays the results obtained from the ANOVA. As expected, P-Values for **n** and **b** are below alpha (0.05), meaning that they have high impact on response variables.

Table 4.6: ANOVA results of Second Model Refinement

Term	Coeff.	SE Coeff.	T-Value	P-Value
Constant	77.00	0.238	323.84	0.00
b	-1.1697	0.0249	-47.03	0.00
n	4.491	0.108	41.40	0.00

For the post processing of the data (Regression Analysis). For this second model refinement, the data obtained in the ANOVA was used to generate the residual plots for heat dissipation percentage in copper wires and temperature of the component. Figures 4.5 and 4.6 display the normal plot of residuals. As mentioned before, this plots are used to confirm that the residuals are normally distributed and that approximately follows a straight line.

In addition, 4.6, shows a better distribution compare to first model refinement, this can attribute to the fact that less input variables were considered.

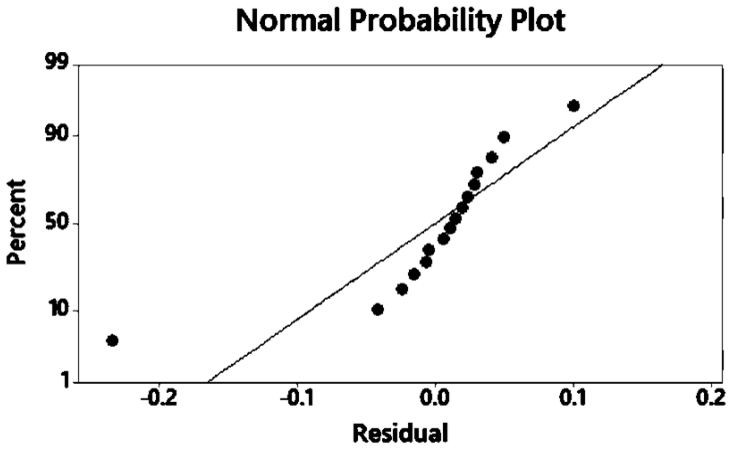

Figure 4.5: Heat dissipation normal probability plot for Second Model Refinement

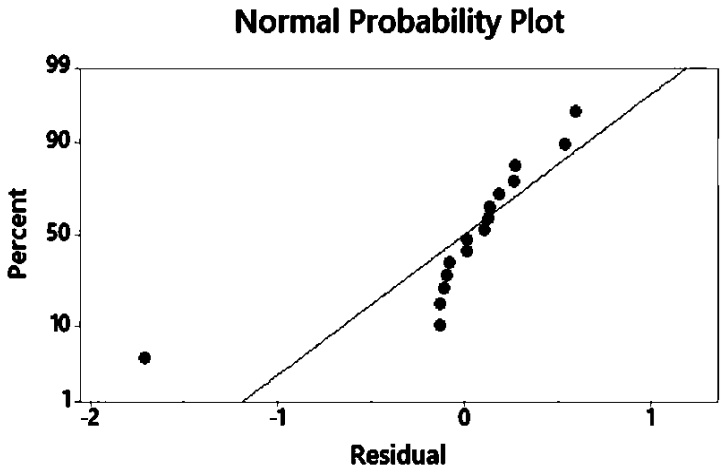

Figure 4.6: Temperature normal probability plot for Second Model Refinement

4.3.3 Third Model Refinement

A third model refinement was considered; nevertheless, new parameters were considered to design this full factorial. On the second model refinement, the analysis of variance showed that **n** and **b** have a positive effect on the responses. However, the normal probability plots started to show certain patterns; which suggests that **n** and **b** are getting normalized. In other words, the value of **b** (0.396) is already too small to consider even smaller values of this variable for further factorial designs. For this reason, new parameters where considered since **b** cannot get any smaller and **n** increases volume fraction considerably. A full factorial Taguchi L-9 was performed. Input parameters were, **h** and **w** done at three levels. Also, the variables **a, b, f**, and **n** were fixed using the values for the best run achieved in second model refinement (see Figure 4.7).

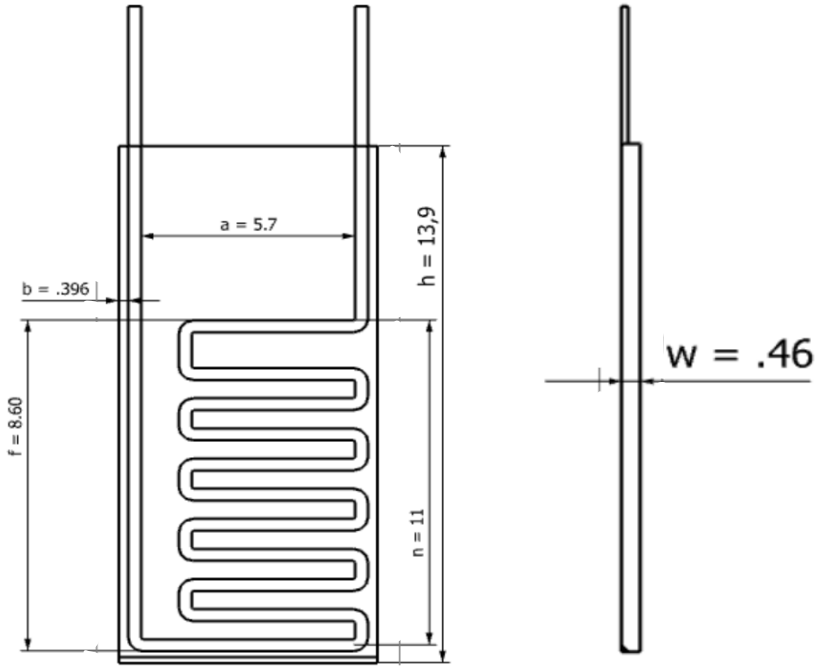

Figure 4.7: Sketch showing input factors h and w with fixed a, b, n and f

Input factors were coded as (1), (2) and (3). Taguchi design L-9 was done with the following configuration: 3^2 and 9 computational runs (see Table 4.8).

Table 4.7: Input variables evaluated at three levels

Factors	High (1)	Standard (2)	Low (3)
w (mm)	1	0.73	0.46
h (mm)	15.933	14.933	13.933

Table 4.8: Nine computational run combinations

Run Number	Factor (input)	
	w	**h**
1	1	1
2	1	2
3	1	3
4	2	1
5	2	2
6	2	3
7	3	1
8	3	2
9	3	3

Same process than the first and second model refinement was performed for the third model refinement. After the nine runs where simulated in Abaqus, the data is analyzed in Minitab to perform an Analysis of Variance. Table 4.9 displays P-Values obtained from ANOVA. These values demonstrate that **w** and **h** also have an impact on response variables since they are smaller than the value of alpha (0.05).

Table 4.9: ANOVA results for Third Model Refinement

Term	Coeff.	SE Coeff.	T-Value	P-Value
Constant	46.33	1.94	23.91	0.00
w	5.142	0.472	10.89	0.00
h	0.785	0.128	6.16	0.00

4.3.4 Fourth Model Refinement

After three model refinements, results showed that; the higher the volume fraction percentage of copper, the higher high dissipation through the deposited copper wires is obtained. In other words, volume fraction has a significant effect over heat dissipation and temperature. For that reason, volume fraction behavior became an important aspect to analyze.

Therefore, a fractional factorial design was performed to understand how heat dissipation increases as volume fraction increases. A Taguchi L12 fractional design was evaluated with the following input factors: (**a, b, n, f, h** and **w**). Moreover, each factor was evaluated at two levels coded as (1) and (2), representing "low" and "high" values, resulting in 12 computational runs. The main goal of this factorial is to obtain a regression equation that will help normalize volume fraction explained in section 4.4.2. In other words, identify the percentage of volume fraction at which starts to normalize and decrease the significance of the response factors (heat dissipation and temperature). Below, Table 4.10 and 4.11 show input factors considered for the fractional design and evaluation levels and the configuration for the 12 computational runs.

Table 4.10: Input factors evaluated at two levels

Factors	Low (1)	High (2)
a (mm)	5.7	9.7
b (mm)	0.396	.73
f (mm)	6.604	8.604
n (number of wire passes)	7	11
h (mm)	11.933	15.933
w (mm)	0.43	1.27

Table 4.11: Twelve computational run combinations

Run Number	Factor (input)					
	a	**b**	**f**	**n**	**h**	**w**
1	1	1	1	1	1	1
2	1	1	1	1	1	2
3	1	1	2	2	2	1
4	1	2	1	2	2	1
5	1	2	2	1	2	2
6	1	2	2	2	1	2
7	**2**	**1**	**2**	**2**	**1**	**1**
8	2	1	2	1	2	2
9	2	1	1	2	2	2
10	2	2	2	1	1	1
11	2	2	1	2	1	2
12	2	2	1	1	2	1

Analysis of Variance (see Table 4.12) showed that variables with P-Values lower than 0.05 are **b, n, h, w**, and VF; however, similar to previous model refinements, f shows no significance and did not appear on the table due it low impact. In addition, Figure 4.8 and 4.9 displays the normal plot of residuals for heat dissipation and temperature. As mentioned before, this plots confirm that residuals are normally distributed since they approximately follow a straight line; therefore, validates the DOEs.

Figure 4.12: ANOVA results for Fourth Model Refinements

Term	Coeff.	SE Coeff.	T-Value	P-Value
Constant	25.93	3.61	7.19	0.001
b	-0.912	0.334	-2.73	0.041
f	-0.680	0.269	-2.53	0.053
n	-4.789	0.481	9.96	0.000
h	-3.475	0.326	-10.67	0.000
w	2.52	1.47	1.72	0.046
VF	1.147	0.302	3.79	0.013

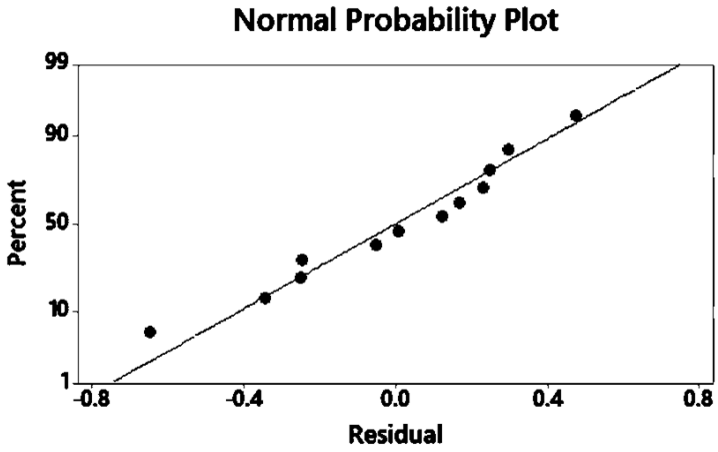

Figure 4.8: Heat dissipation normal probability plot for Fourth Model Refinement

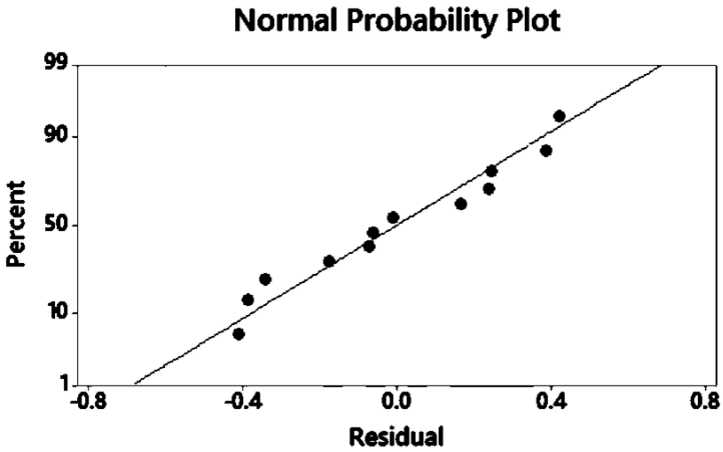

Figure 4.9: Temperature normal probability plot for Fourth Model Refinement

4.3.5 Fifth Model Refinement

Results obtained with the fourth model refinement, demonstrate that heat dissipation percentage did not increase considerably when the volume fraction was increase by more than 7%. Therefore, a final model refinement using fractional factorial design Taguchi L-8 was considered with the intent to comprehend how volume fraction behaves with volume fraction higher than 10%. For this design, factors that showed higher influence in ANOVA where chosen as the input variables; these include **(n, b** and **w).** Input variables where analyzed at two level coded as (1) and (2). Taguchi Design L-8 was done with the following configuration: 2^3giving a total of eight computational runs as shown in Table 4.13.

Figure 4.13: Eight computational run combinations

Run Number	Factor (input)		
	n	**b**	**w**
1	1	1	1
2	1	1	2
3	1	2	1
4	1	2	2
5	2	1	1
6	**2**	**1**	**2**
7	2	2	1
8	2	2	2

Results showed what expected: The higher the volume fraction, an increase in heat dissipation will occur. However, heat dissipation increments in percentage are increasing relatively slow even if volume fraction increasing by more than 17%. For this reason, after conducting five model refinements, and a total of 54 computational runs. The behavior of Heat Dissipation and Temperature vs. Volume fraction were plotted for all runs. In other words, all factorial designs

were plotted to see the performance of heat dissipation and temperature having different volume fractions. As shown in Figure 4.10 Heat Dissipation vs. Volume Fraction; heat dissipation through copper wires increases considerably when having a volume fraction ranging from 1.5% to 7% approximately. However, when volume fraction increase more than 7%, (VF) starts to lose impact as shown in the figure. On the other hand, Figure 4.11 displays the normal plot of residuals of the 54 computational runs. This plot confirms that residuals are normal distributed since it has the tendency to follow the straight line as shown.

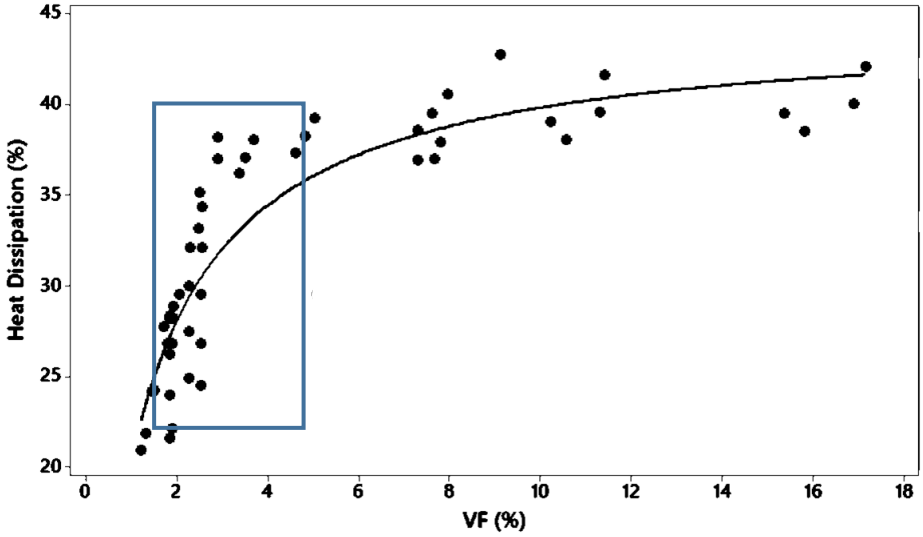

Figure 4.10: Heat dissipation vs. Volume Fraction

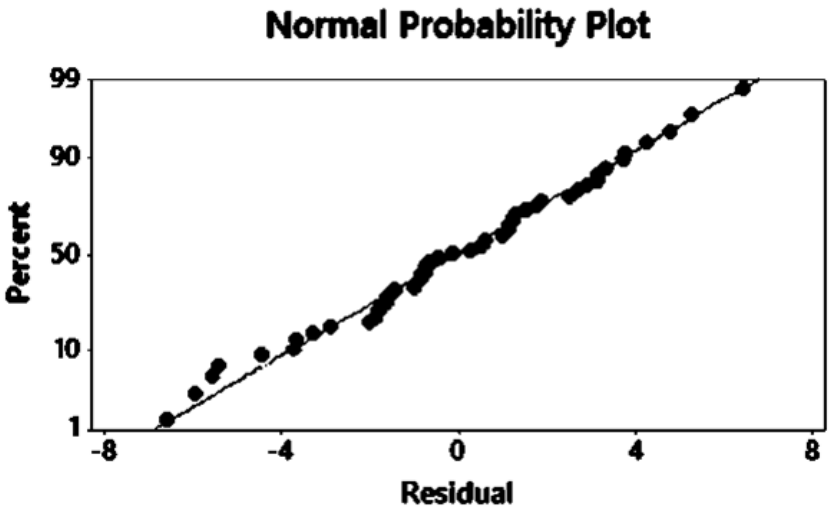

Figure 4.11: Heat dissipation normal probability plot for all Model Refinements

Nonetheless, in Figure 4.12 showing Temperature vs. Volume Fraction; temperature remains constant with a volume fraction of 2% and higher. This can be contributed to the fact that; temperature cannot drop below room temperature. Figure 4.13, which displays the normal plot of residuals for all the simulations performed, confirms that temperature does not follow a normal distribution, since the temperature cannot drop below room temperature.

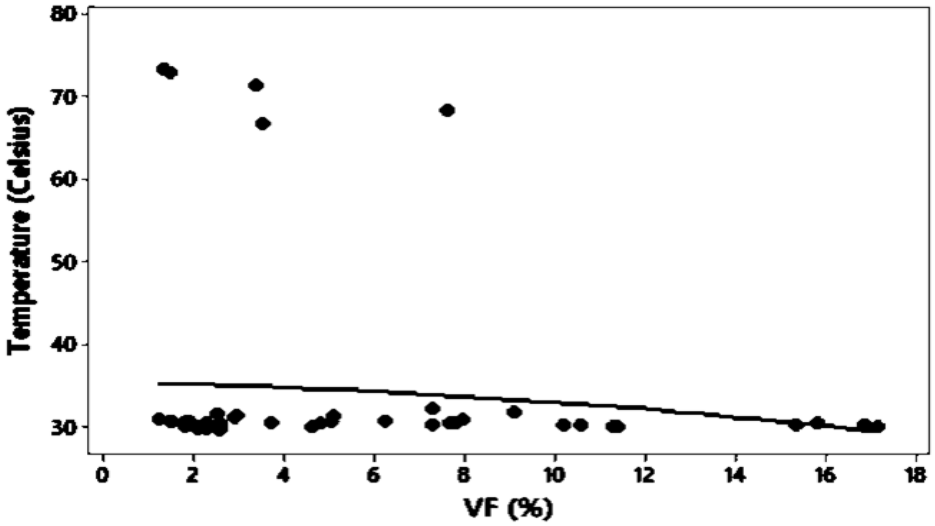

Figure 4.12: Temperature vs. Volume Fraction

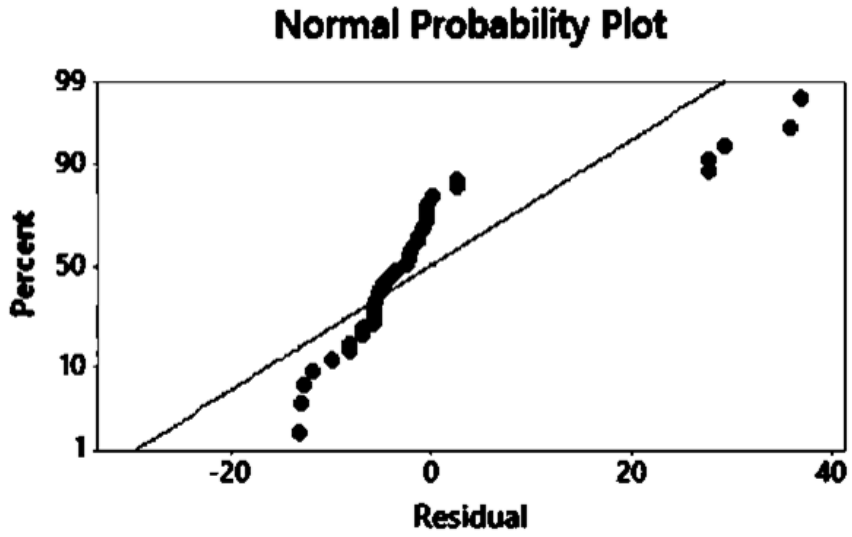

Figure 4.13: Temperature normal probability plot for all Model Refinements

4.4 Constrained Optimization

4.4.1 Overview

Based on the results obtained; simulations showed that as volume fraction increases, heat dissipation percentage increases as well. However, data in Figure 4.10 suggests that volume fraction does not have a linear behavior; compare to the input variables previously used. In addition, after volume fraction is increased more than 7%, this variable starts to lower its significance over the response variables. In other words, heat dissipation and temperature starts to have little improvement when having volume fractions higher that 7% compare to lower percentages. Being that said, the objective of this section is to develop an algorithm that will optimize the existent design using a constrained volume fraction. In other words, this algorithm will allow to find the optimum input variable combination that will give a high heat dissipation percentage in deposited wires and a low temperature in the component.

As discussed in previous sections; optimization refers to the improvement of the performance of a system in order to obtain the maximum benefit from it using different methods such as RSM optimization. This section on the other hand, seeks to find an "optimal" output and express it as a numerical value, this is called a mathematical optimization; which is widely used in the areas of engineering design. There is a lot of techniques to achieve a mathematical optimization, but in general, all techniques follow the same concept. Mathematical optimization techniques, consist in having an objective function and a set of constraints expressed in the form of a system of equations or inequalities. This optimization differs from traditional optimization which goal is to find global optima; on the other hand, mathematical optimization looks to obtain an optimization using constraints [43]. In other words, a function is either maximized or minimized relative to a given set of alternatives called feasible region or constraint region. The constraint region is taken to be a subset of $\mathbb{R}^n$ (real n-dimensional space) and the objective function is a function from $\mathbb{R}^n$ to $\mathbb{R}$ [44].

4.4.2 Objective Function

The objective function is a mathematical equation that describes the response with respect of input variables. In a constrained problem, the objective function minimizes or maximizes a numerical value. Also, it is an indicator on how much the independent variables (design parameters) contributes to the response (Heat dissipation through additional copper wires and Temperature). The objective function takes the following general form:

$$c_1x_1 + c_2x_2 + \cdots + c_nx_n \tag{4-1}$$

Where x_n represent the input variables $x = \{a,\ b,\ n,\ f,\ w,\ h \ldots vf\}$ and c_n are the constant coefficients or multipliers that describe the size of the effect the independent variables are having on your dependent variable. To obtain an objective function, a regression analysis was performed in section 4.3.4. In this section, the first part was to perform a fractional design of experiments Taguchi L12. Afterwards, the ANOVA determined the relationship of the input and output factors; this analysis will discard the input variables without impact on the response from the objective function. Finally, the regression analysis found that the connection between the independent and dependent variables is linear logarithmic. For this reason, the following linear regression equation was generated by the data obtained during Taguchi L12. This linear equation will allow to optimized the responses with a constrained optimization. As mentioned before, the coefficients of the objective function indicate the contribution to the value of the objective function of one unit of the corresponding variable

$$h(x) = 50.75 + 1.1331n - 4.202b - 1.246h - 3.694w - 0.3417a - 0.0180vf \tag{4-2}$$

4.4.3 Constraint Optimization with Lagrange Multipliers

The first approach to perform a mathematical optimization was a constrained optimization using Lagrange Multipliers. This optimization minimizes $H(s)$, subject to the condition $g(s) = 0$, where s are the input factors or design variable *i.e.* $s = \{a, n, w, h, f \ldots vf\}$. The objective function (4-2) was obtained from the equation generated in the linear regression performed in the fourth

model refinement (Taguchi L-12). This equation describes heat dissipation behavior. In addition, a constrained equation (4-13) was developed to express volume fraction as a function of the design factors including volume fraction f

$$\mathrm{H}(s) = \mathrm{H}(s_1, s_2, s_3, \ldots . s_n) \tag{4-3}$$

$$\mathrm{g}(s) = vf(a, n, w, h) - f = 0 \tag{4-4}$$

Hence, to minimize $H(s)$ follows the following: Find s such that $H(s)$ is minimized and $\mathrm{g}(s) = 0$. To achieve this, the idea is to find point where the gradient vectors H and g are parallel to each other. This process consists on setting the gradient of a certain function, called the Lagrangian equal to the zero vector [46]. In other word, by adding an additional variable (Lagrange multiplier) to the (s_n) factors that creates the following Lagrangian Function: where λ is the Lagrange multiplier [47].

$$L(s, \lambda) = H(s) - \lambda[g(s) - f] \tag{4-5}$$

The constraint optimization problem consists on finding the critical points of $L\ in\ \mathbb{R}^n$ .More specifically, let find a point (s, λ) such that:

$$\nabla L(s, \lambda) = \begin{bmatrix} \nabla_x L(s, \lambda) \\ \nabla_\lambda L(s, \lambda) \end{bmatrix} = \begin{bmatrix} \nabla h(s) + \sum_{i=1}^{n} \nabla g_i\,(s) \\ g_1(s) \\ \vdots \\ g_n(s) \end{bmatrix} \tag{4-6}$$

equals zero. This will give an equation with (n) number of variables; to solve this, an iterative method is commonly used. Where the objective function and the constrained equation are differentiated twice to find the root of the multivariable problem [48].

$$s_{t+1}, \lambda_{t+1} = (s_t, \lambda_t - \nabla^2 L(s_t \lambda_t)^{-1} \nabla L(s, \lambda) \tag{4-7}$$

Then, Hessian of the Lagrangian is given by the following matrix

$$\nabla^2 L(x,\lambda) = \begin{bmatrix} \nabla^2 h(s) + \sum_{i=1}^{n} \nabla^2 g_i\,(s) \cdots \nabla g_1(s) \ldots \nabla g_n(s) \\ \nabla g_1(s)^T \quad \vdots \\ \vdots \quad 0 \\ \nabla g_n(s)^T \quad \vdots \end{bmatrix} \tag{4-8}$$

MATLAB was used to iterate and solve the unknowns by Newton-Raphson scheme iterate. *MATLAB A1. And A2. codes are attached in Appendix

while |r| > TOL
compute J
solve J * ds = - r for ds
s = s + ds
compute r

end while. [47]

4.4.4 Linear Programming Constraint Optimization

After running the code for solving the constrained problem using Lagrange multipliers, the results obtained where not feasible *i.e.* negative values. For this reason, a second approach was made, by taking into consideration that equations are linear; also, more constraints were included. The second mathematical optimization performed in this section is said to be linear and will be solve through linear programming. Linear programming optimizes over the real n-dimensional space where the objective function is a linear function. The constraint region is the set of solution to a finite number of linear inequalities, equalities or bounds constraints of form [44]:

$$a_1 x_1 + a_2 x_2 + \cdots + a_n x_n \leq b_i \qquad i = 1, \ldots, s \tag{4-9}$$

$$c_1 x_1 + c_2 x_2 + \cdots + c_n x_n = b_i \qquad i = s+1, \ldots, n \tag{4-10}$$

$$l \leq x \leq u \tag{4-11}$$

4.4.4.1 Linear Programming Problem Formulation

The first step to formulate an optimization problem is to identify the input variables or independent factors. As discussed in previous sections, the analyzed independent factors where the dimensions of the design. RSM methodology process, helped identify which input factors (x) have the most beneficial impact on the responses (Y). For this mathematical optimization, independent variables are (**a, b, n, w, h** and **VF**). Note that volume fraction is now considered as an input variable instead of a response variable. Once the input variables are identified, the next step is to define the objective function that will be minimize. In section 4.4.2 the definition and the procedure to get the objective function is explained. As mention in this section, a design of experiments Taguchi L-12 was performed using six input factors including (**a, b, f, n, w**, and **h**); however, for the linear regression, VF was used as the seventh input factor since we wish to optimized the design having a limit for VF. The performed linear regression created a regression equation that will serve as the objective function for the constrained linear optimization. The following formula represents the objective function obtained from the linear regression performed in Minitab with a Taguchi L12 design.

$$h(x) = 50.75 + 1.1331n - 4.202b - 1.246h - 3.694w - 0.3417a - 0.0180v \quad (4\text{-}2)$$

The next step is to define the constraints. Constrains are known to be the relations between input variables and response variables. A set of constraints allows some of the input variables to take on certain values and exclude other *i.e*. a constraint is applied so all dimensions are positive; otherwise it would not make sense to have negative input variables. For this optimization problem two types of constraints will be use: Equalities and bounds. The equality constraint equation was developed to normalize volume fraction. In other words, the equality constraint equation has the following form:

$$\frac{v_{wire}}{v_{polycarbonate}+v_{wire}} \cdot 100 = vf \quad (4\text{-}12)$$

Where:

$v_{wire} = Total\ volume\ of\ deposited\ copper\ wire.$

$v_{polycarbonate} = Total\ volume\ of\ the\ polycarbonte\ block.$

The equation was developed in terms of input variables; in other words, this formula describes volume of copper wires and polycarbonate in terms of (a, b, n, …w), that creates a *volume fraction constraint* equation. The following equation shows the expanded volume fraction equation*:*

$$g(x) = 2 \cdot h - n + \left(\frac{28vf}{5}\right) + a \cdot n + 2 \cdot h \cdot vf + n \cdot vf - a \cdot n \cdot vf - a \cdot h \cdot vf \cdot w - 2 \cdot b \cdot h \cdot vf \cdot w + \frac{38}{5} \quad (4\text{-}13)$$

Lastly, bound constraints are defined considering the input parameters used in the design of experiments. Bound constraints are widely used in constrained optimization problems because, many algorithms tend to give "undesirable results" *i.e.* negative values. For this reason, bounds are used to give a range of solutions to the input variables. The following equations where used as bound constraints for the linear optimization:

$$5 \leq a \leq 10 \quad (4\text{-}14)$$

$$0.4 \leq b \leq 0.8 \quad (4\text{-}15)$$

$$7 \leq n \leq 25 \quad (4\text{-}16)$$

$$0.73 \leq w \leq 1.27 \quad (4\text{-}17)$$

$$14 \leq h \leq 17 \quad (4\text{-}18)$$

$$4 \leq vf \leq 7 \quad (4\text{-}19)$$

Hence, the final set up for the linear constrained optimization is the following:

$Minimize$:

$$h(x) = 50.75 + 1.1331n - 4.202b - 1.246h - 3.694w - 0.3417a - 0.0180vf \quad (4\text{-}2)$$

$Subjected\ to$:

$$\rightarrow g(x) = 2 \cdot h - n + \left(\frac{28vf}{5}\right) + a \cdot n + 2 \cdot h \cdot vf + n \cdot vf - a \cdot n \cdot vf - a \cdot h \cdot vf \cdot w - 2 \cdot b \cdot h \cdot vf \cdot w + \frac{38}{5} \quad (4\text{-}13)$$

$$\rightarrow 5 \leq a \leq 10 \quad (4\text{-}14)$$

$$\rightarrow 0.4 \leq b \leq 0.8 \quad (4\text{-}15)$$

$$\rightarrow 7 \leq n \leq 25 \quad (4\text{-}16)$$

$$\rightarrow 0.73 \leq w \leq 1.27 \quad (4\text{-}17)$$

$$\rightarrow 14 \leq h \leq 17 \quad (4\text{-}18)$$

$$\rightarrow 4 \leq vf \leq 7 \quad (4\text{-}19)$$

Linear programming problem will find the point that minimizes h(x) yet, satisfy the constraints that create the feasible regions.

4.4.4.2 Linear Programming with MATLAB

As explained in previous section, the main goal of this optimization process is to find the values of the input variables that minimize the objective function while satisfying the constraints that will give an "optimal solution" [43]. It is known that there are widely developed algorithms to optimize problems. However, for this optimization problem, linear programing with MATLAB was used since both the objective function and the constraints are in linear. The command to optimize the constraint problem is ***linprog*** command. The command linprog from the optimization toolbox, implements the algorithm to solve a linear program with the following form [45]. *MATLAB code will be attached in Appendix

$$\min f * x$$

$$\text{Subject to } A * x \leq b$$

Where f is any vector and the matrix A and the vector b define the linear constraints. Giving the following:

$$\min \quad 50.75 + 1.1331n - 4.202b - 1.246h - 3.694w - 0.3417a - 0.0180vf$$

$$subject\ to:$$

$$\begin{cases} 2 \cdot h - n + \left(\frac{28vf}{5}\right) + a \cdot n + 2 \cdot h \cdot vf + n \cdot vf - a \cdot n \cdot vf \\ \qquad -a \cdot h \cdot vf \cdot w - 2 \cdot b \cdot h \cdot vf \cdot w + \frac{38}{5} \\ 5 \leq a \leq 10 \\ 0.4 \leq b \leq 0.8 \\ 7 \leq n \leq 25 \\ 0.73 \leq w \leq 1.27 \\ 14 \leq h \leq 17 \\ 4 \leq vf \leq 7 \end{cases}$$

As a summary, this section explained the process employed for a constrained optimization. This process can be summarized in the following:

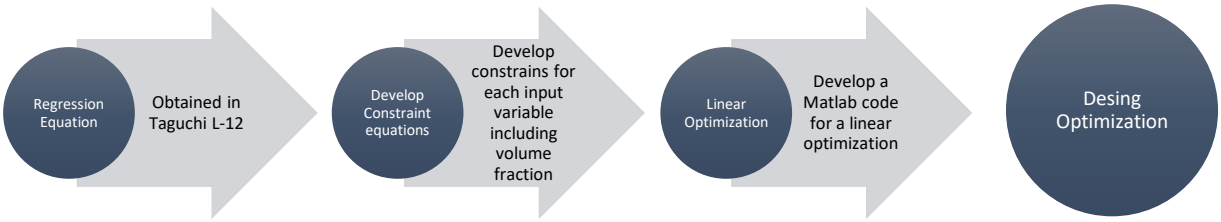

5. Results and Discussion

5.1 Overview

This chapter will explain in detail the best result obtained in the (FEA) thermal simulations in Abaqus for every model refinement. In other words, when a design of experiments was conducted, a computational run obtained the highest dissipation percentage through deposited copper wire. Then, the following model refinement was made considering results in previous and so on. In addition, section 5.7 will provide the result obtained with the linear constrained optimization. In other words, a simulation will be performed using the optimum input variables that will give a high dissipation percentage having a constrained volume fraction ranging from 4 to 7%.

5.2 First Model Refinement

For first model refinement, a fractional factorial design was performed to collect data as part of the optimization process. The factorial design was chosen to identify the significance on suggested input variables. In addition, four input variables (**a, b, n**, and **f**) were evaluated at two levels "low" and "high" giving a 2^{4-1} form of fractional factorial design. Therefore, giving a combination of eight computational simulation.

Table 5.1 shows the results obtained at each computational run. This table is divided in three mayor sections. The first section shows the number of simulation, second section shows the input factors considered as well as the combination used; final section shows the response outputs which includes: the percentage of heat dissipated through deposited copper wires, maximum temperature (Celsius) of the 3D printed component with heating joule and the Volume Fraction for the additional copper wires. As shown in table, best results were obtained in Run 5 with the combination code (2), (2), (1) and (1) for **a, b, f** and **n** respectively. The percentage of heat dissipated through deposited copper wires is 29.53% with a maximum temperature of 29.85 ℃ and a copper volume fraction of 2.052%

Table 5.1: Results at each computational run for First Model Refinement

Run Number	Factor (input)				Response (output)		
	a	b	f	n	Heat (y_1) %	Temp (y_2) ℃	Volume Fraction (y_3) %
1	2	2	2	2	26.85	30.05	1.797
2	1	2	2	1	27.75	30.35	1.722
3	2	1	2	1	24.23	30.55	1.502
4	1	1	2	2	20.93	30.95	1.199
5	**2**	**2**	**1**	**1**	**29.53**	**29.85**	**2.052**
6	1	2	1	2	24.17	30.65	1.471
7	2	1	1	2	21.86	73.45	1.315
8	1	1	1	1	24.16	72.95	1.444

5.2.1 Thermal FEA Results

After the eight different combinations of the fractional factorial design were simulated; the *.inp file was modified for each run to create a new *.dat files. As discussed before, the generated *.dat file, displays the total heat dissipated through the deposited copper wires as well as the heat dissipated through polycarbonate. This process allows to get the percentage to heat dissipated through the wires displayed in Table 5.1.

In addition, the results for the run that obtained a higher percentage of heat dissipation are displayed below (Run5). Figures 5.1 and 5.2 displays RFLE11 values of the polycarbonate block with additional deposited copper wire at different angles. RFLE11, accounts for the total heat flux out ($^{W}/_{mm^3}$) by convection surfaces. As observed, negative or low values of RFLE11 represents that most of the heat is being dissipated though these surfaces. On the other hand, higher numbers suggest that less heat is going through those surfaces. The main goal of the design optimization is to dissipate great amounts of heat through the deposited copper wires. In other words, to achieve this, deposited copper wires should display low values of RFLE11. Figure 5.1 shows that approximately $-4.725e^{-1}\ W/mm^3$ are being dissipated through this surfaces. On the other hand,

Figure 5.2 displays the total heat flux out from polycarbonate ranging from $-2.006e^1\ to\ -6.349\ e^0.W/mm^3$. Therefore, a great amount of heat is still being dissipated through polycarbonate.

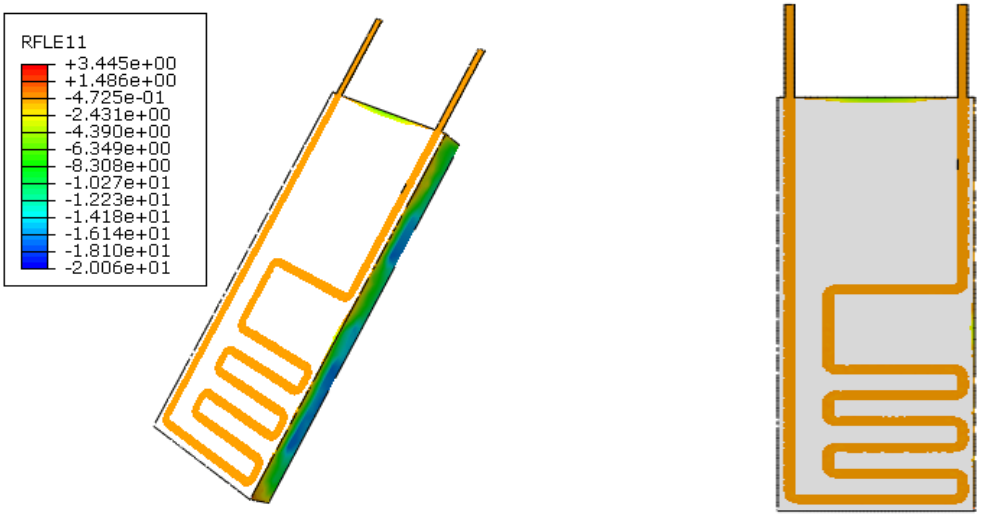

Figure 5.1: Total Heat Flux out from deposited copper wire for First Model Refinement

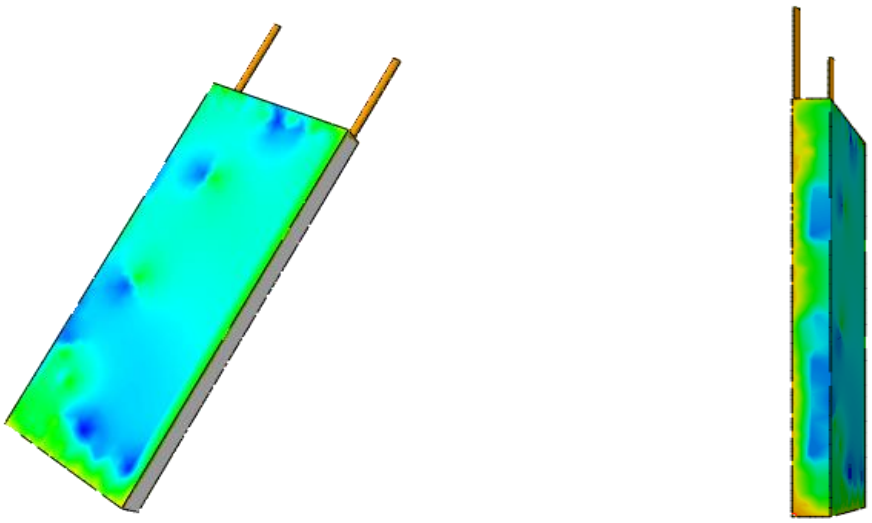

Figure 5.2: Total Heat Flux out from polycarbonate for First Model Refinement

Next, Figure 5.3 show temperature profile NT11 which shows a maximum temperature of 303 kelvins. In comparison to the first design that was simulated using deposited copper wires, the temperature decrease 74.71%. In addition, temperature is now within safe operating temperature range for electronics.

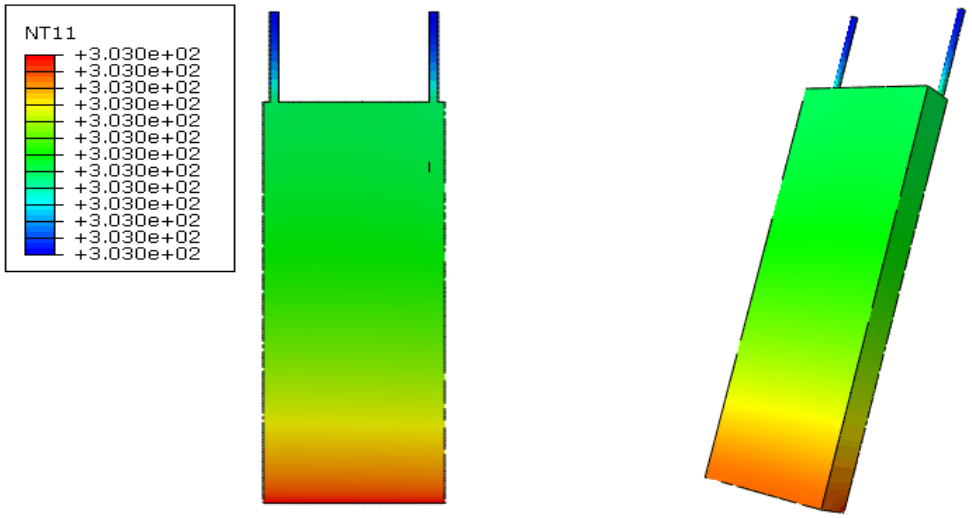

Figure 5.3: Temperature profile for First Model Refinement

5.3 Second Model Refinement

After the Analysis of variance was performed for the first model refinement, it was found that a and f does not have a significant effect over the responses. For that reason, a full factorial design Taguchi L-16 with form 4^2 was conducted using n and b as input factors, and evaluated at four levels. These variables were chosen since they show high impact on the responses during ANOVA. Therefore, sixteen combinations of dimensions of n and b were simulated in Abaqus. Table 5.2 displays the results obtained in this factorial design. Highest percentage of heat dissipation was achieved at run number 4 having a combination of (1), (4) for n and b respectively. Results showed that 34.33% of the total heat generated by joule heating was dissipated through the deposited copper wires. In addition, temperature decrease by a small percentage compare to the first model refinement, giving 29.55℃ as the maximum temperature.

Table 5.2 show the results obtained in the sixteen runs performed. The table is divided in three main sections. The first section shows the number of simulation, second section shows the input factors considered as well as the combination used; final section shows the response outputs which includes: the percentage of heat dissipated through deposited copper wires, maximum temperature (Celsius) of the 3D printed component with heating joule and the Volume Fraction for the deposited copper wires.

Table 5.2: Results at each computational run for Second Model Refinement

Run Number	Factor (input)		Response (output)		
	n	**b**	**Heat** (y_1) **%**	**Temp** (y_2) ℃	**Volume Fraction** (y_3) **%**
1	1	1	28.24	30.25	1.84
2	1	2	28.85	30.15	1.91
3	1	3	32.13	29.75	2.28
4	**1**	**4**	**34.33**	**29.55**	**2.56**
5	2	1	26.25	30.35	1.84
6	2	2	26.82	30.35	1.90
7	2	3	29.97	29.95	2.27
8	2	4	32.08	29.75	2.56
9	3	1	23.98	30.55	1.84
10	3	2	24.53	30.45	2.54
11	3	3	27.5	30.15	2.27
12	3	4	29.53	29.85	2.54
13	4	1	21.64	30.75	1.83
14	4	2	22.15	30.65	1.90
15	4	3	24.93	30.35	2.26
16	4	4	26.83	30.05	2.54

5.3.1 Thermal FEA Results

Figures below displays the results for the run that achieved the highest heat dissipation through deposited wires (Run 4). In addition, the results for the run that obtained a higher percentage of heat dissipation are displayed below. Figure 5.4 displays the values for total heat flux out by convection surfaces ($^{W}/_{mm^3}$). The displayed RFLE11 values show that approximately $-8.121e^{-1}\,W/mm^3$ are being dissipated through deposited copper wires. In addition, Figure 5.5 displays the total heat flux out from polycarbonate. As shown by the color code, small sections have a RFLE11 of $-9.309e^{0}$; on the other hand, larger areas show heat flux out of $-6.123\,e^{0}.W/mm^3$. In addition, Figure 5.6 displays the temperature values obtained in the simulation. The maximum temperature obtained was 302.7 Kelvins; in comparison with first model refinement, temperature decrease by a small percentage.

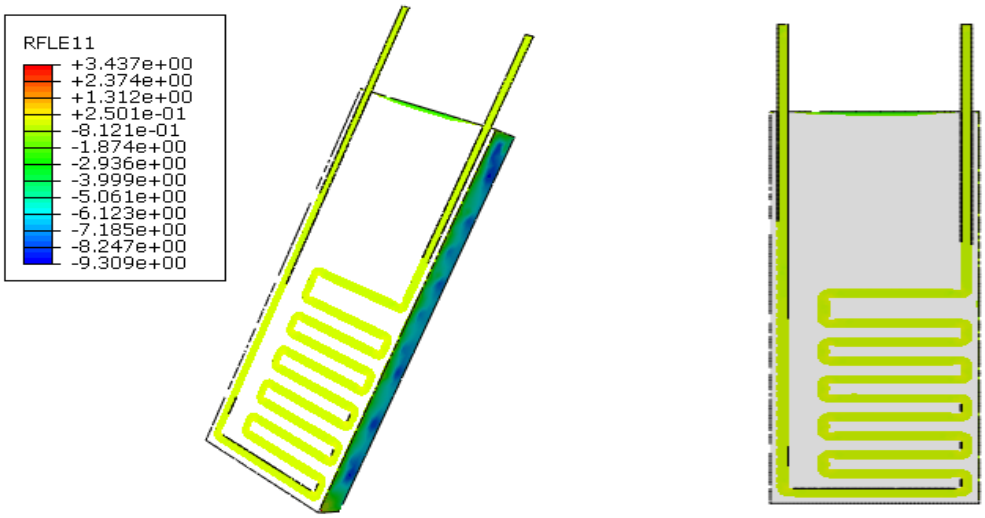

Figure 5.4: Total Heat Flux out from deposited copper wire for Second Model Refinement

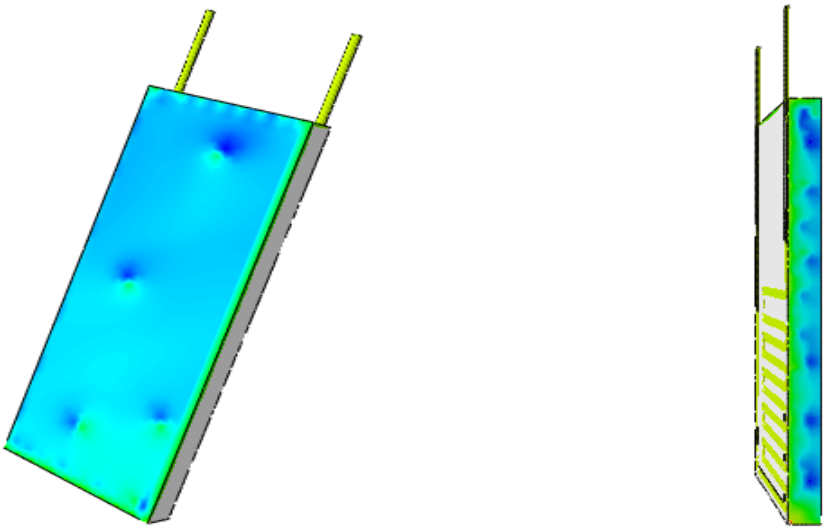

Figure 5.5: Total Heat Flux out from polycarbonate for Second Model Refinement

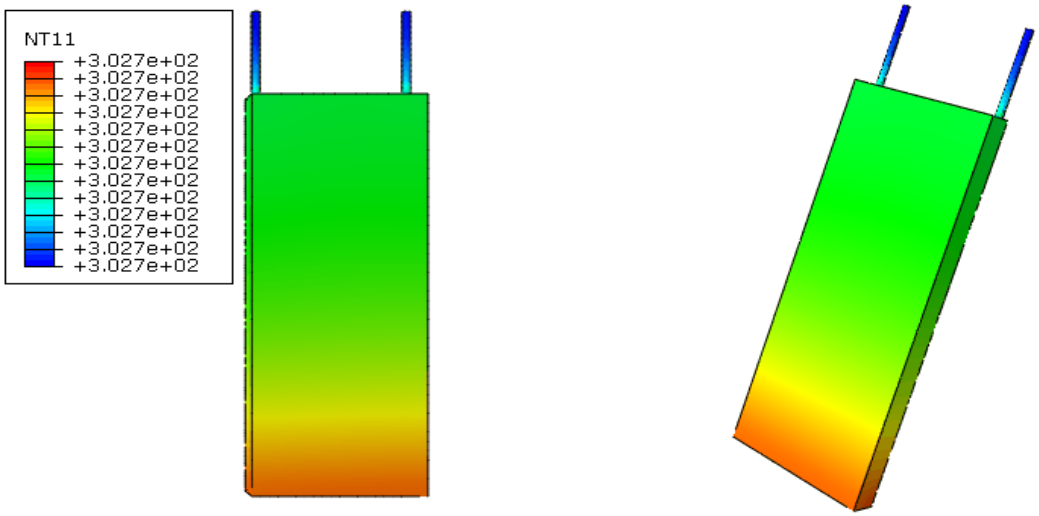

Figure 5.6: Temperature profile for Second Model Refinement

5.4 Third Model Refinement

As explained in section, new parameters were considered for the third model refinement. This is because, the analysis of variance performed in the second model refinement suggested that b and n were getting normalize; in other words, they started to lose effect over the responses.

Therefore, two new variables **w** and **h** were taken into consideration and evaluated with a full factorial Taguchi L-9 design of experiments. Input variables where evaluated at three levels giving a total of nine computational runs. Table 5.3 shows the results obtained during this design; the combination of input factors that gave a higher percentage of heat dissipation through deposited wires was run 9. The combination used is (3), (3) for w and h respectively, giving a total of 40.53% of heat dissipated through the wires and a maximum temperature of 30.85 ℃.Table 5.3 is divided in three sections as explained with previous model refinements, showing the results (output) obtained at each run that was simulated.

Table 5.3: Results at each computational run for Third Model Refinement

Run Number	Factor (input)		Response (output)		
	w	h	Heat (y_1) %	Temp (y_2) ℃	Volume Fraction (y_3) %
1	1	1	36.18	71.35	3.37
2	1	2	37.08	66.75	3.51
3	1	3	38.02	30.45	3.68
4	2	1	37.33	30.05	4.61
5	2	2	38.26	30.35	4.81
6	2	3	39.23	30.65	5.03
7	3	1	38.56	30.25	7.30
8	3	2	39.52	68.25	7.61
9	**3**	**3**	**40.53**	**30.85**	**7.96**

5.4.1 Thermal FEA Results

Results for the run that obtained a higher percentage of heat dissipation are displayed below. Figure 5.7 displays the values for total heat flux out by convection surfaces ($^{W}/_{mm^3}$). The displayed RFLE11 values show that approximately $-1.288e^0\ W/mm^3$ are being dissipated through deposited copper wires. In addition, Figure 5.8 displays the total heat flux out from

polycarbonate. As shown by the color code, “blue” sections in polycarbonate are smaller than past model refinements; RFLE11 value for this sections is $-1.080e^1$. In addition, larger sections in polycarbonate are getting “greener” showing a heat flux out of $-2.501\, e^0. W/mm^3$. In other words, these figures demonstrate that heat flux out is starting to be evenly distributed in the model; considering that, RFLE11 values for polycarbonate do no differ much from RFLE11 values for the deposited copper wire.

In past model refinements, RFLE11 values for polycarbonate where much lower compare to RFLE11 values of the deposited wires. In addition, Figure 5.9 displays the temperature values obtained in the simulation. The maximum temperature obtained was 304.0 Kelvins; in comparison with second model refinement, temperature increased. This can be attributed to the fact that copper volume fraction increased considerably (7.96%); therefore, temperature increased slightly.

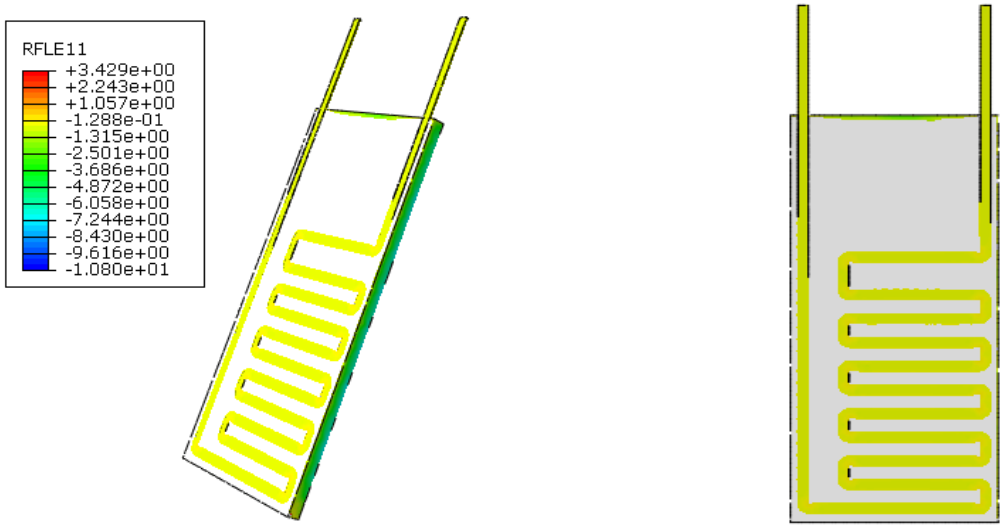

Figure 5.7: Total Heat Flux out from deposited copper wire for Third Model Refinement

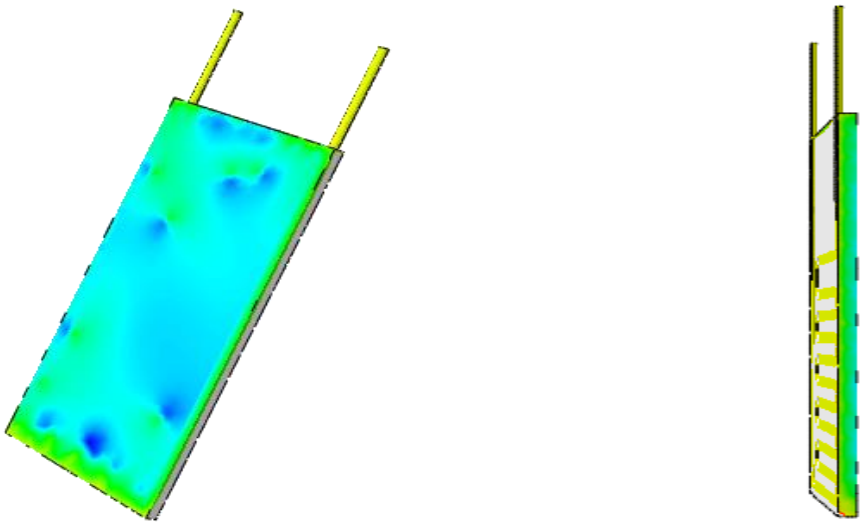

Figure 5.8: Total Heat Flux out from polycarbonate block for Third Model Refinement

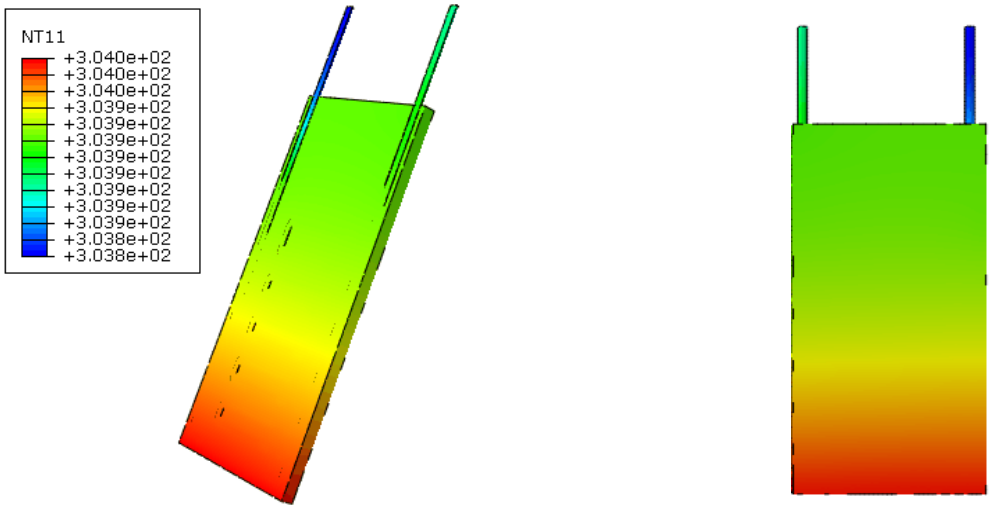

Figure 5.9: Temperature profile for Third Model Refinement

5.5 Fourth Model Refinement

Results showed after model refinements that, heat dissipation increases when copper volume fraction is increased too. In other words, volume fraction has a significant impact on

response variables. For this reason, a fractional factorial design was conducted in order to understand volume fraction behavior. A Taguchi L-12 design was chosen to understand how heat dissipation increases as the volume fraction increase. This design evaluated the input factors (**a, b, n, f, h** and **w**).at two levels, giving a total of twelve computational runs. Table 5.4 displays the results obtained at each run divided by: percentage of heat dissipation, maximum temperature and percentage of copper volume fraction. Run seven showed the highest heat dissipation, having a combination of (2), (1), (2), (2), (1) and (1) for **a, b, n, f, h** and **w** respectively. 42.73% of total heat was dissipated through the deposited wires, with a maximum temperature of 31.65℃ with a copper volume fraction of 9.11%.

Table 5.4: Results at each computational run for Fourth Model Refinement

Run Number	Factor (input)						Response (output)		
	a	**b**	**f**	**n**	**h**	**w**	**Heat** (y_1) **%**	**Temp** (y_2) ℃	**Volume Fraction** (y_3) **%**
1	1	1	1	1	1	1	36.9	32.25	7.29
2	1	1	1	1	1	2	33.13	31.45	2.48
3	1	1	2	2	2	1	37.89	30.35	7.81
4	1	2	1	2	2	1	36.97	30.45	7.68
5	1	2	2	1	2	2	28.24	30.35	1.91
6	1	2	2	2	1	2	37.00	31.15	2.90
7	**2**	**1**	**2**	**2**	**1**	**1**	**42.73**	**31.65**	**9.11**
8	2	1	2	1	2	2	28.34	30.55	1.83
9	2	1	1	2	2	2	35.15	30.05	2.51
10	2	2	2	1	1	1	33.72	30.75	6.21
11	2	2	1	2	1	2	38.20	31.35	2.91
12	2	2	1	1	2	1	29.56	31.25	5.08

5.5.1 FEA Thermal Results

Run 7, which obtained the highest percentage of heat dissipation is displayed below. Figure 5.10 displays the values for total heat flux out from the deposited copper wires. Values of RFLE11 show that approximately $1.377e^0\,W/mm^3$ are being dissipated through deposited copper wires. In addition, Figure 5.11 displays the total heat flux out from polycarbonate. As discussed in previous model refinements, color code "blue" suggest high heat flux getting out from these surfaces. For this run, bluish are sections in polycarbonate are getting larger. This can be attributed to the fact that, when having volume fraction higher than 9%, this variable starts to lose effect over response variables. However, values are lower than previous model refinements, RFLE11 values for the bluish sections ranges from $-7.508e^0 to -3.700e^0$. Additionally, Figure 5.12 displays the temperature values obtained in the simulation. The maximum temperature obtained was 304.8 Kelvins. As well as previous model refinement, temperature increased since volume fraction of copper is getting higher (9.11%); therefore, temperature increased slightly.

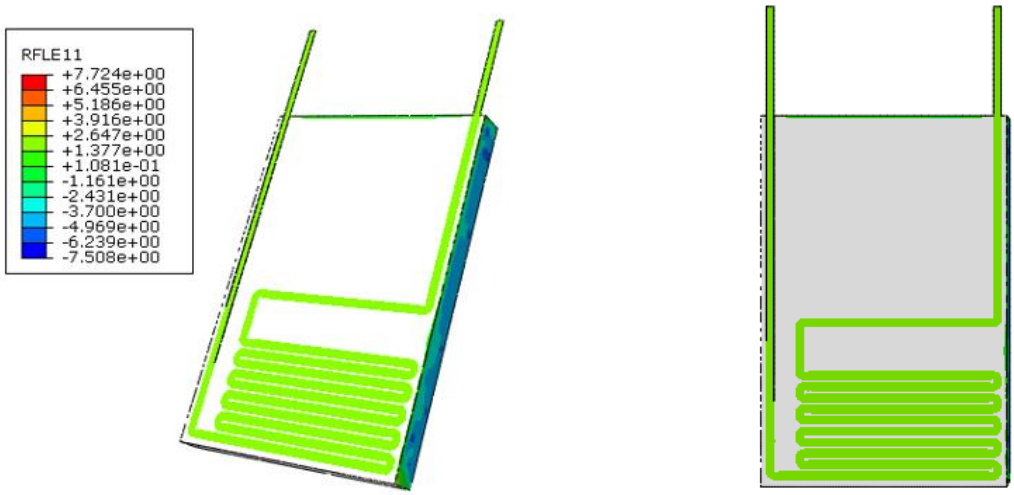

Figure 5.10: Total Heat Flux out from deposited copper wire for Fourth Model Refinement

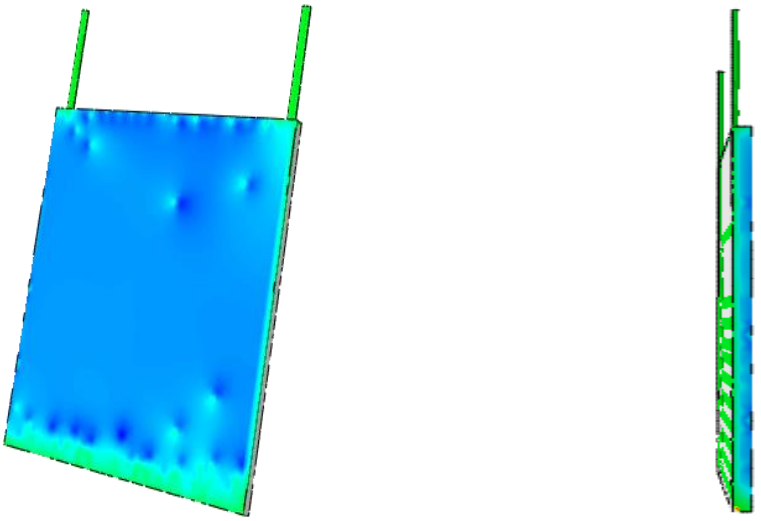

Figure 5.11: Total Heat Flux out from polycarbonate block for Fourth Model Refinement

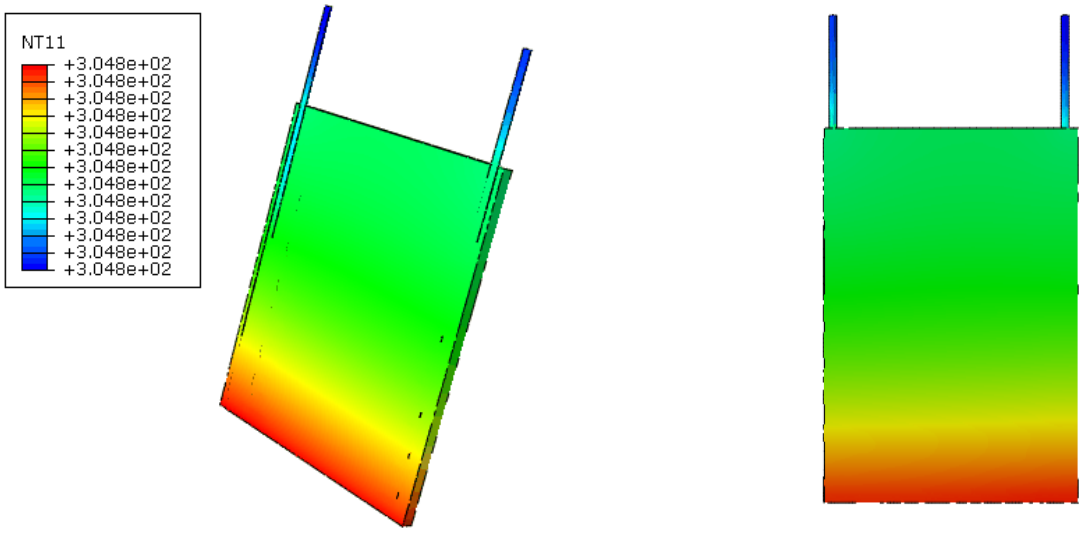

Figure 5.12: Temperature profile for Fourth Model Refinement

5.6 Fifth Model Refinement

As discussed in section, and as observed in previous results, heat dissipation percentage does not increase by much when volume fraction is increased by more than 7%. In fact, when volume fraction of copper is more than 7% it starts to have a negative effect on temperature, since

it starts to present a slight increase. Therefore, a final model refinement using fractional factorial design Taguchi L-8 was considered with the intent to comprehend how volume fraction behaves with volume fraction higher than 10%. For this design, the input variables considered where: (**n, b** and **w)**, analyzed at two level, giving eight computational runs. Table 5.5, displays the results obtain at each run. Run 6 obtained the highest percentage in heat dissipation through deposited copper wires with a combination of (2), (1) and (2) for **n, b** and **w** respectively. Run six, obtained a percentage of 42.0840% of heat dissipated through deposited wires, a maximum temperature of 29.95 ℃ and a volume fraction of 17.15%.

Table 5.5: Results at each computational run for Fifth Model Refinement

Run Number	Factor (input)			Response (output)		
	n	b	w	Heat (y_1) %	Temp (y_2) ℃	Volume Fraction (y_3) %
1	1	1	1	39.5655	30.05	11.2944
2	1	1	2	40.0431	30.15	16.9011
3	1	2	1	38.0152	30.25	10.5650
4	1	2	2	38.4777	30.35	15.8141
5	2	1	1	41.5972	29.95	11.4074
6	**2**	**1**	**2**	**42.0840**	**29.95**	**17.1554**
7	2	2	1	39.0276	30.15	10.2135
8	2	2	2	39.4827	30.25	15.3589

5.6.1 FEA Thermal Results

Run 6 obtained the highest percentage of heat dissipation and results are displayed below. Figure 5.13 displays the values for total heat flux out from deposited copper wires. Values of RFLE11 show that approximately $-6.452e^{1}\,W/mm^{3}$ are being dissipated through deposited copper wires. In addition, Figure 5.14 display the total heat flux out from polycarbonate. As shown in this figures, polycarbonate is getting "greenish" colors ranging from $-6.452e^{0} to\ 4.819e^{-1}$. In

other words, these figures demonstrate that heat flux out is evenly distributed in the model; considering that, RFLE11 values for polycarbonate do no differ much from RFLE11 values for the deposited copper wire; however, this is also attributed to the fact that volume fraction increased considerably. However, this is not considered a good design since the measurements are too small to be manufactured. Additionally, Figure 5.15 display the temperature values obtained in the simulation. The maximum temperature obtained was 303.1 Kelvins.

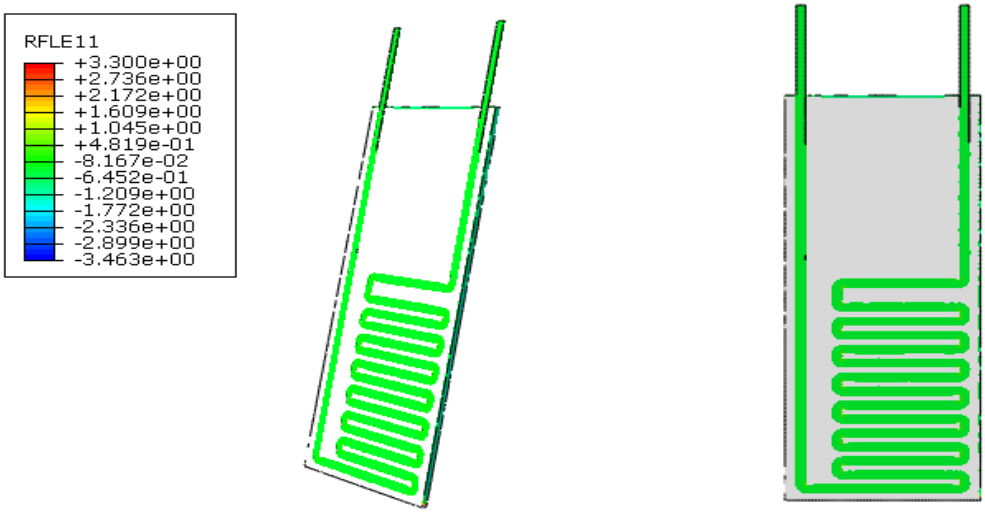

Figure 5.13: Total Heat Flux out from deposited copper wire for Fifth Model Refinement

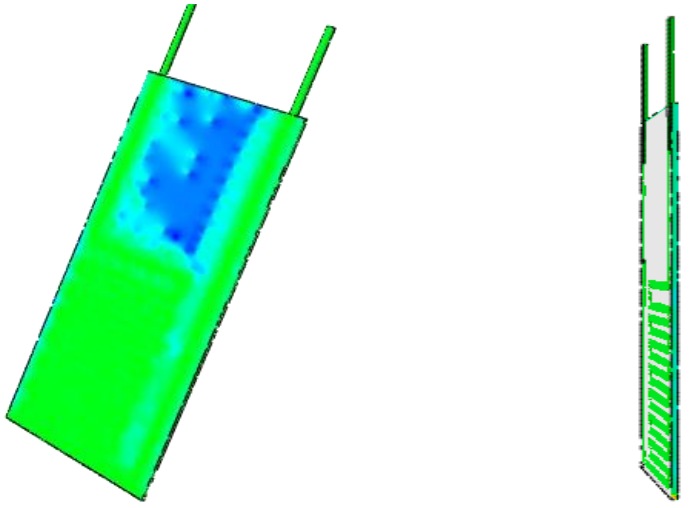

Figure 5.14: Total Heat Flux out from polycarbonate for Fifth Model Refinement

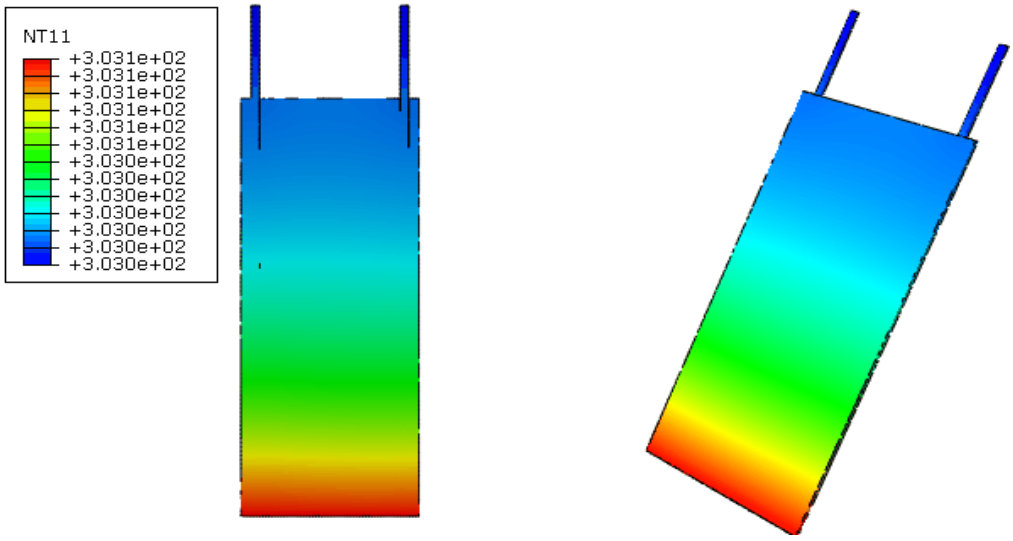

Figure 5.15: Temperature profile for Fifth Model Refinement

5.7 Constrained Optimization

As discussed in section 4.4.5, a MATLAB code was created to solve the linear constrained optimization problem. This code solved for the for x_n (design parameters) that minimizes the objective function $f(x)$ (Metamodel function obtained from Taguchi L-12)

In other words, this code gave the optimum parameters to achieve a high percentage of heat dissipation through the deposited copper wires and an overall low temperature in the 3-D printed component. After the MATLAB code created to solve a linear constrained problem was run, it gave thus six parameters. The following Table 5.6 displays the results obtained for each input parameter.

Table 5.6: Results for each input variable obtained through MATLAB code

Design Parameters (Input Variables)	Optimal Dimension
a	10 mm
b	0.80 mm
n	25 (Number of passes)
w	1.27 mm
h	14 mm
VF	7%

5.7.1 FEA Thermal Results

A final computational simulation was conducted in Abaqus, using the dimensions obtained from the MATLAB code. Figure 5.16 displays the values for total heat flux out. Values of RFLE11 show that approximately $-6.108e^{-2}\,W/mm^3$ are being dissipated through deposited copper wires. This value, is the lowest value for RFLE11 achieved among all simulations performed. In addition, Figure 5.17 displays the total heat flux out from polycarbonate. As shown, polycarbonate show small sections having the lowest values of RFLE11 $-7.448e^{0}$. However, larger sections are showing greater values of RFLE11 values ranging from $-5.601e^{0} to\ 1.908e^{0}$. In other words, these figures demonstrate that heat flux out is evenly distributed in the model; considering that, RFLE11 values for polycarbonate do no differ much from RFLE11 values for the deposited copper wire. Additionally, Figure 5.18 displays the temperature profile, having 302.4 Kelvins as the maximum temperature. In addition to the simulation, the *.inp file was modified to create a new *.dat file, to calculate the total heat dissipated through the additional deposited wire. Table 5.7 display the total heat dissipated through the wires, maximum temperature and the wire volume fraction. As observed, linear optimization obtained the highest percentage of heat dissipated

through deposited wires among all simulations performed; while maintaining a low volume fraction and temperature.

Table 5.7: Results of the computational run for linear optimization

Linear Optimization	Factor (input)					Response (output)		
	a	**b**	**n**	**w**	**h**	**Heat** (y_1) **%**	**Temp** (y_2) ℃	**Volume Fraction** (y_3) **%**
1	10	0.8	25	1.27	14	50.43	29.25	4.69

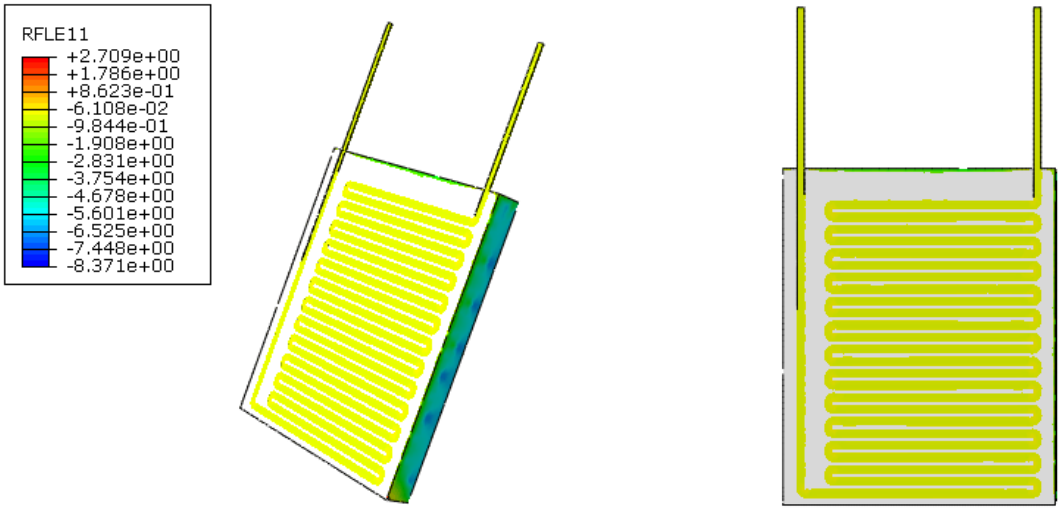

Figure 5.16: Total Heat Flux out from deposited copper wire for Linear Optimization

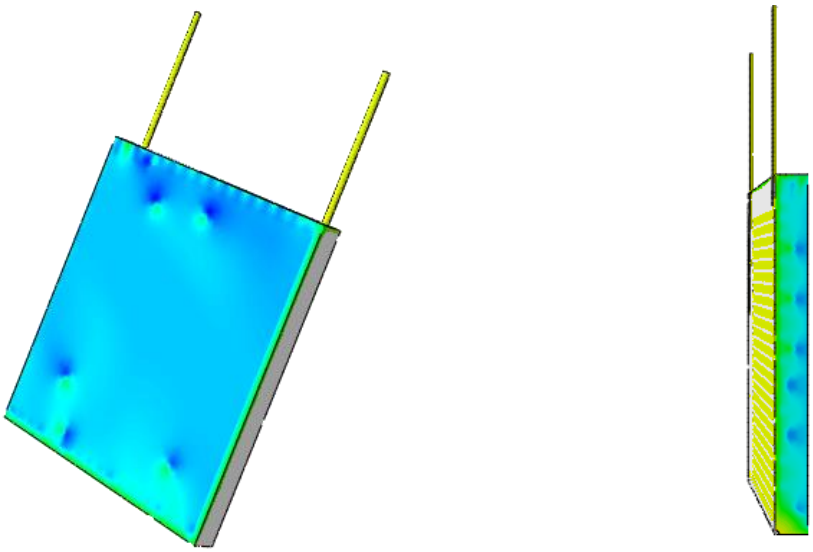

Figure 5.17: Total Heat Flux out from polycarbonate for Linear Optimization

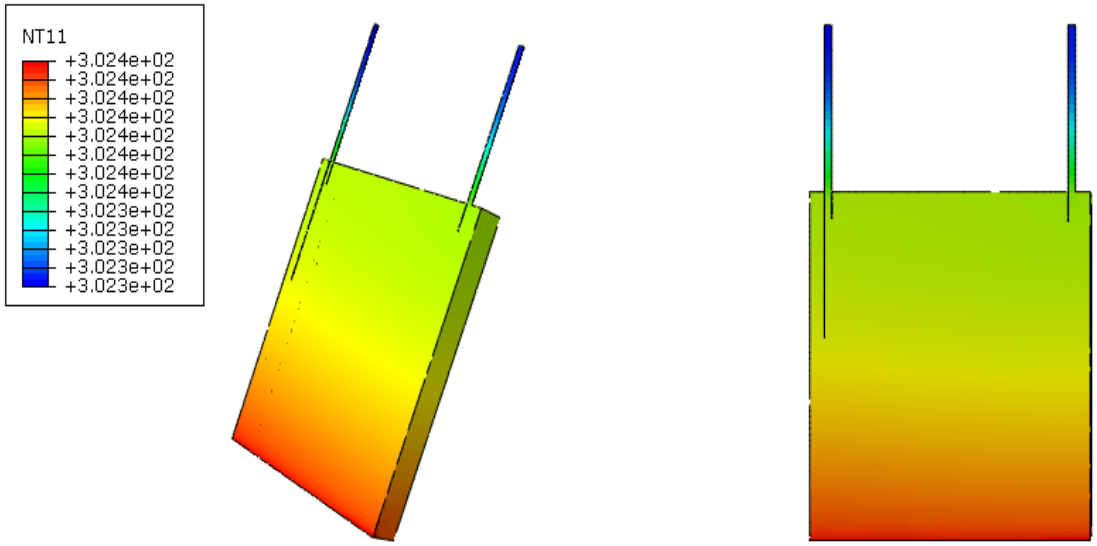

Figure 5.18: Temperature profile for Linear Optimization

6. Conclusions

6.1 Summary

The industry of additive manufacturing (AM) has become a subject of constant reinvention; in fact, one emerging application of AM is focused on creating 3D printed parts with embedded electronics. As this application of AM continues to innovate by creating complex embedded electronic components, thermal management is of particular interest since high power densities and size reduction of electronic components has led to an overheating issue. In other words, electronic components operating above "safe operating temperatures" decreases considerably its reliability leading to a premature failure.

In this study, a polycarbonate component design with integral electrical circuitry that is fabricated by Material Extrusion process was considered. After Finite Element Analysis was conducted to analyze the joule heating effect, results where the following:

- Maximum temperature of 62.65 ℃

In addition to copper deposited in the FDM process for the circuitry, complementary copper was deposited to help conduct the heat generated by the joule effect. FEA results where the following:

- First Model Refinement design using **a, b, n**, and **f** as input factors showed the following results after a thermal FEA was conducted:
  - 29.53% of total heat was dissipated through the deposited copper wires
  - 29.85 ℃ was the maximum temperature of the electrical component
  - 2.052% Copper volume fraction
- Second Model Refinement using **n** and **b** as input factors showed the following results after a thermal FEA was performed:
  - 34.33% of total heat was dissipated through the deposited copper wires
  - 29.55 ℃ was the maximum temperature of the electrical component

    - 2.56% Copper volume fraction
- Third Model Refinement using **w** and **h** as input factors showed the following results after a thermal FEA was performed: 5
    - 40.53% of total heat was dissipated through the deposited copper wires
    - 30.85 ℃ was the maximum temperature of the electrical component
    - 7.96% Copper volume fraction
- Fourth Model Refinement using **a, b, n, f, h** and **w** as input factors showed the following results after a thermal FEA was conducted:
    - 42.73% of total heat was dissipated through the deposited copper wires
    - 31.65℃ was the maximum temperature of the electrical component
    - 9.11% Copper volume fraction
- Fifth Model Refinement using **b, n**, and **w** as input factors showed the following results after the thermal FEA was conducted:
    - 42.08% of total heat was dissipated through the deposited copper wires
    - 29.95 ℃ was the maximum temperature of the electrical component
    - 17.15% Copper volume fraction
- Linear optimization shows the following results after a FEA was performed
    - 50.43% of total heat was dissipated through the deposited copper wires
    - 29.25 ℃ was the maximum temperature of the electrical component
    - 4.69% Copper volume fraction

This guided methodology optimized the model by effectively increasing heat dissipation through the additional copper wire. The optimized model with additional deposited copper wire dissipated 50.43% of the total heat generated, whereas, previous design dissipated only 9.49% of the total heat generated by the joule heating; also, temperature was lowered from 118.05 ℃ to 29.25 ℃ degrees. That is, an increase in percentage of the heat dissipated through the additional deposited wires by 81.1 and a decrease of the overall temperature of the component by 75.2%.

In addition, the first three model refinements suggested that volume fraction was the main contributor to the increase in heat dissipation; as percentage continued to increase as the volume fraction got higher. However, after the fourth model refinement, it was observed that the change in heat percentage from third to fourth model refinement was not as large as the change in percentage of copper volume fraction. Therefore, a fifth model refinement was conducted to analyze the behavior of volume fraction. Volume fraction was increased from 9.11% (fourth model refinement) to 17.15% (fifth model refinement) giving an increment of in VF of 8.04%. However, heat dissipation did not show an increase in percentage as expected; in fact, it showed a decrease of .06%. These results, confirmed that, when volume fraction is higher than 7%, it loses effect over the response. On the other hand, linear optimization achieved the highest percentage of heat dissipation (50.43%) having a 4.96% of copper volume fraction. MATLAB code showed that volume fraction was going to be 7%; the difference can be attributed to the fact that, the constrained equation for volume fraction did not consider the curvature of copper wire at each pass (n).

6.2 Research Contributions

Many Research studies have attempt to address thermal management issue in traditional electronics, mainly through heat sinks, phase change material (PCM)-based cooling system and heat pipe cooling mechanisms, and most of these systems cooled by forced convection. Nonetheless, few research studies have been reported on overheating in 3D printed embedded electronics. Results obtained in this research have introduced new findings that will benefit the field of embedding electronics in AM parts. The main research contributions of this work are as follows:

- Finite Element model to simulate heat generation and maximum temperature.
- Dissipate heat generated by joule heating effect though natural convection.
- Increase of heat dissipation by 81.1% compared to first design with deposited copper wires.
- Lowered the temperature of the 3D printed embedded electronic by 75.2%

6.2.1 Proposed Research Applications

Also, the methodology followed to optimize a response during this study can be applied to cooling or heating systems such as thermoelectric. Explained more in detail, these systems undergoes the thermoelectric effect; which is defined as the direct conversion of temperature differences to electric voltage and vice versa [56]. The thermoelectric effect encompasses three different phenomena including [57]:

- Seebeck effect
- Peltier effect
- Thomson effect.

A significant amount of energy we consume each year is rejected as waste heat to the ambient. Optimization studies have been performed to determine the effect of system size, exhaust and coolant flow conditions, and thermoelectric material on the net gains produced by the Thermoelectric system and on the optimum system design [58]. Therefore, Finite Element Analysis and Response Surface Methodology can be applied to optimize response variables:

- Increase electrical energy produced from heat waste

That is influenced by the following independent or input factors:

- Design parameters (That will determine the optimum system size and design)
- Thermoelectric materials
- Exhaust and coolant flow conditions

6.3 Future Work

The W.M Keck Center for 3D Innovation, located at the University of Texas at El Paso, is a laboratory dedicated to advanced manufacturing technology. As explained throughout this study, AM fabricated 3D structures with complex geometries. The Keck Center focuses on research to enhance this technology to include the ability to print multifunctional structures i.e. Embedded electronics [49]. The W.M Keck Center, will start to fabricate some of the suggested designs in this study. Manufacturing will be through Material Extrusion process which is based on an

extrusion process. Then, the fabricated components will be tested by applying voltage and analyzing the behavior of the component fabricated.

References

[1] C. B. Williams, F. Mistree and D. W. Rosen, “Towards the design of a layer-based additive manufacturing process for the realization of metal parts of designed mesostructured” The G.W. Woodruff School of Mechanical Engineering, p. 1-2, 2005.

[2] Yong Huang and Ming C. Leu, “Frontiers of Additive Manufacturing Research and Education” NS. F Additive Manufacturing Workshop, pp.6-24, 2014

[3] Ian Gibson, David Rosen and Brent Stucker, “Additive Manufacturing Technologies 3d Printing, Rapid Prototyping and Direct Digital Manufacturing” Springer Verlag, pp. 12-25, 2016. Print.

[4] Strayasys.com, “FDM Technology: 3D print durable parts with real thermoplastic” 2017. [Online] Available: http://www.stratasys.com/3d-printers/technologies/fdm-technology [Accessed: 11-April-2017].

[5] Elizabeth Palermo, “Fused Deposition Modeling: Most Common 3D printing Method” [Online] Live Science, September, 2013 [Accessed: 11-April-2017].

[6] R.S Khandpur, “Printed Circuit Boards: Design, Fabrication and Assembly” New York: McGraw Hill Professional, First Edition, pp. 34-50, 2006.

[7] J. O’Donnell, F. Ahmadkhanlou, Hwan-Sik Yoon, G. Washington, “All printed smart structures: a viable option?” Dept. of Mechanical and Aerospace Engineering, vol. 9057, pp. 3-6, 2014.

[8] Comsol.com, “The Joule Heating Effect” [Online] Available: https://www.comsol.com/multiphysics/the-joule-heating-effect, [Accessed: 13-April-2017].

[9] D. Espalin, D. W. Muse, E. MacDonald and R. B. Wicker, “3D Printing Multifunctionality: structures with electronics.” Int J Adv Manuf Technol, 72: 963. doi:10.1007/s00170-014-5717-7, (2014).

[10] E.C. Mikkelson, “Characterization and Modeling of the Thermal Properties of Photopolymers for Material Jetting Processes” Virginia Polytechnic Institute and State University, pp.6-7, 2014.

[11] Kos, A and Mey G, “Thermal Modelling and Optimization of Power Microcircuits” Electromechanical Publications Ltd, 1997.

[12] Computerhope.com “Heat Sink” [Online] Available: http://www.computerhope.com/jargon/h/heatsink.htm, [Accessed: 12-April-2017]

[13] Hambley, Allan R. “Electrical Engineering: Principles and Applications” Pearson, pp. 50-65, 2014.

[14] Bhatti et al. “High Performance heat sink for electronics cooling” Delphi Technologies, Inc, pp. 1-10, 2001.

[15] Z. J. Zuo, M.T. North and K.L. Wert, “High Heat Flux Heat Pipe Mechanism for Cooling of Electronics” Inter Society Conference of Thermal Phenomena. pp. 122-128, 2000.

[16] Chun Lung et al. “Application of heat pipe for cooling inside electric vehicle” The Hong Kong Polytechnic University, 2011.

[17] A. Bhattacharya and R.L. Mahajan, “Finned Metal Foam Heat Sinks for Electronics Cooling in Forced Convection” Journal of Electronic Packaging, Vol. 124, pp. 155-161, 2002.

[18] N. C. Gallego and J.W. Klett, “Carbon foams for thermal management” Carbon Materials Technology Group, Vol 41, issue 7, pp. 1461-1466, 2003.

[19] W. Escher, B. Michel and D. Poulikakos, “A novel high performance, ultra-thin heat sink for electronics” International Journal of Heat and Fluid Flow, Volume 31, Issue 4, pp. 586-598, 2010.

[20] Ying-Che Weng et al. “Heat pipe with PCM for electronic cooling” Applied energy, Volume 88, Issue 55, pp. 1825-1833, 2011.

[21] K. Namba et al. “Heat Pipes for Electronic Devices Cooling and Evaluation of their thermal performance” Inter Society Conference on Thermal Phenomena, pp: 456-459, 1998.

[22] Phasechange.com “What exactly are phase change materials and how do they work?” [Online] Available: http://www.phasechange.com/how-it-works/, [Accessed: 4-April-2017]

[23] Azeem Anzar, Shine K, “Transient Thermal Analysis of Phase change material based heat sinks” International Journal of Research in Engineering and Technology, pp. 703-712, 2013.

[24] Yunus A. Cengel, “Heat and Mass transfer: A practical approach” Third Edition, Ch 2. Heat Conduction Equation pp 63-66, 2002.

[25] Incropera, DeWitt, Bergman and Lavine,” Fundamentals of Heat and Mass Transfer” Wiley Sixth Edition, Ch. 3. One-Dimensional, Steady-State Conduction, pp. 125-137, 1998.

[26] Umsl.edu “Joule Heating of a Resistor” [Online] Available: http://www.umsl.edu/~physics/files/pdfs/Electricity%20and%20Magnetism%20Lab/Exp6.JouleHeating.pdf [Accessed: 13-April-2017]

[27] Stanislaw Olszewski, “Quantum Aspects of the Joule-Lenz Law” Journal of Modern Physics, pp: 162-174, 2015.

[28] Tan and Tso, “Cooling of mobile electronic devices using phase change materials” Applied thermal engineering, Volume 24, Issues 2-3, pp: 159-169, 2004.

[29] 3dprinting-bloc.com “ABS advantages” [Online] Available: http://3dprinting-blog.com/tag/abs-advantages/ [Accessed: 14-April-2017]

[30] Rodriguez F., Cohen C, Ober C, “Principles of Polymer Systems” Taylor & Francis, New York, London, 2003.

[31] Seshasayee Nikhil, “Understanding Thermal Dissipation and Design of a Heatsink” Application Report, Texas Instruments, pp: 1-4, May 2011.

[32] Professionalplastics.com, “Thermal Properties of Plastic Materials” [Online] Available: http://www.professionalplastics.com/professionalplastics/ThermalPropertiesofPlasticMaterials.pdf [Accessed: 14-April-2017]

[33] ABAQUS/CAE Users' Guide (6.14), Dassault Systems, 2014.

[34] Altairuniversity.com “2D Meshing” [Online] Available: http://www.altairuniversity.com/wp-content/uploads/2014/02/2Dmeshing.pdf [Accessed: 21-April-2017]

[35] Mishra Rajeev, “The Temperature Ratings of Electronic Parts” Design, Materials, compounds, Adhesives, Substrates, Number 1, Semiconductor & Measurement, Volume 10, pp: 1-10, February 2004

[36] Burkhardt Jochen, “Parametric optimization and parameter studies” Fraunhofer Institute of Manufacturing Engineering and Automation IPA, pp: 1, 2016.

[37] Khuri Andre I and Mukhopadhyay Siuli, “Response Surface Methodology” Wiley Interdisciplinary Reviews: Computational Statistics, Volume 2, Issue 2, pp: 128-149, April 2010.

[38] Public.iastate.edu, “Multivariate Linear Regression Models” [Online] Available: http://www.public.iastate.edu/~maitra/stat501/lectures/MultivariateRegression.pdf [Accessed: 27-April-2017]

[39] Cardinal R. N and Aitken M. R. F. “ANOVA for the behavioral sciences researcher” Mahwah, NJ: Lawrence Erlbaum Associates, 2006.

[40] Bezerra Almeida, Erthal Santelli, et. Al., “Response Surface Methodology (RSM) as a tool for optimization in analytical chemistry” Talanta, Volume 76, Issue 5, pp: 159-977, 2008.

[41] Lundstedt, Seifert, et. Al., “Experimental design and optimization” Chemometrics and Intelligent Laboratory Systems, Volume 42, Issue 1-2, pp: 3-40, 1998.

[42] Support.minitab.com, “Interpret the key results for One-Way ANOVA” [Online] Available: http://support.minitab.com/en-us/minitab-express/1/help-and-how-to/modeling-statistics/anova/how-to/one-way-anova/interpret-the-results/key-results/ [Accessed: 27-April-2017]

[43] Arsham, Hossein, “Deterministic Modeling: Linear Optimization with Applications” University of Baltimore, pp 1-20, 2005.

[44] Boyd, Stephen, “Convex Optimization” Department of Electrical Engineering, Stanford University, pp: 1-4, 2004

[45] Verschelde, Jan, “Linear Programming in MATLAB” Introduction to Symbolic Computation MCS 320, pp: 1-3, 2007

[46] Khanacademy.com “Lagrange multipliers, Introduction” [Online] Available: https://www.khanacademy.org/math/multivariable-calculus/applications-of-multivariable-derivatives/constrained-optimization/a/lagrange-multipliers-single-constraint [Accessed: 27-April-2017].

[47] Chessa, Jack F. “Lagrange Multipliers” University of Texas at El Paso, pp: 1-2, 2017

[48] Hauser, Kris, “Constrained Optimization, Lagrange Multipliers and KKT Conditions” Semantic Scholar, Allen Institute for Artificial Intelligence, pp: 1-9, February, 2002.

[49] keck.utep.edu “Advanced additive manufacturing applications” [Online] Available: http://keck.utep.edu/index.php?option=com_content&view=article&id=11&Itemid=113 [Accessed: 31-April-2017]

[50] Kerns, Jeff “Powder-Metallurgy Processes” Machine design, pp: 1-5, July 28, 2016

[51] Suk-Joong L. Kang, “Sintering, Densification, Grain Growth, and Microstructure” Butterworth-Heinemann, Technology & Engineering, pp: 20-24, 2004

[52] Saylor.org “The Sintering Process” [Online] Available: https://www.saylor.org/site/wp-content/uploads/2013/01/ME203-4.3-Sintering.pdf [Accessed: 13-May-2017]

[53] Tu, W. and T. Pollock, “Modeling Deformation Mechanisms and Grain Structure Evolution during Forging of Powder-Metallurgy Nickel-Base Turbine Disk Alloy”. Minerals, Metals and Materials Society, February, 2011.

[54] Bandar Al-Mangour, “Powder metallurgy of stainless steel: State-of-the art, challenges, and development” Nova Science Publishers, Machinability of SLM processed MMC, pp: 40-44, January, 2015

[55] Neuforce.com “Stainless Steel Metal Injection Molding and Sintering Techniques Revolutionize the production of Barbed Stainless Steel Hose Fittings” [Online] Available: http://www.neuforce.com/Downloads/StainlessSteel_Sintering.pdf [Accessed: 13-May-2017]

[56] Tudi.com “Advantages of Thermoelectric Systems in Heating and Cooling” [Online] Available: http://www.tudi.com/advantages-thermoelectric-systems-heating-cooling [Accessed 14-May-2017]

[57] M. Wagner, “Simulation of Thermoelectric Devices-Fundamentals of Thermoelectric devices” Institute of Microelectronics, pp: 3-8, July 1979

[58] Karri A, Madhav, “Thermoelectric power generation system optimization studies” Clarkson University pp: 57-60, January, 2011

Nomenclature

AM	Additive Manufacturing
ABS	Acrylonitrile butadiene styrene
ANOVA	Analysis of Variance
CAD	Computer Aided Design
DOE	Design of Experiments
FEA	Finite Element Analysis
FEM	Finite Element Method
FDM	Fused deposition modeling
LOM	Laminated object manufacturing
NT11	Temperature Profile
PC	Polycarbonate
PLA	Polylactic Acid
PCB	Printed circuit boards
RFLE11	Total Heat flux out
RSM	Response Surface Methodology
SL	Selective laser sintering
STL	Stereolithography
VF	Volume Fraction
A	Area
β	Coefficient of volume expansion, (1/K)
cp	Specific heat
d	Diameter
Gr_L	Grashof number
g	Gravitational acceleration (m/s^2)
h	Heat transfer coefficient
I	Current
J	Jacobian Matrix
J	Joule
K	Kelvin

kg	Kilogram
l	Length
L_c	Characteristic length of the geometry, (m)
m	Meters
mm	Millimeters
$\overline{Nu_L}$	Nusselt number
P_r	Prandtl number
P	Power
q_w	Heat flux
r	Radius
r_o	Outer radius
r_i	Inner radius
Ra_L	Rayleigh number
$\mathbb{R}^n$	Real n-dimensional space
R	Resistance
$\dot{s}$	Joule heating per unit length
T_{max}	Maximum temperature
T_f	Film temperature
T_∞	Ambient temperature
T_s	Temperature of the surface(℃)
V	Voltage
W	Watts
$\dot{\Delta}$	Heat generation
ΔV	Pressure drop
φ	Resistivity
ρ	Density
α	Thermal expansion
λ	Lagrange Multiplier
κ	Thermal conductivity
ϑ	Kinematic viscosity of the fluid, (m^2/s)

Appendix A

MATLAB code (.M file)

A MATLAB code implemented to solve a constrained optimization problem with Lagrange Multipliers is shown below. Code A1. Finds Hessian Matrix. Code A2. Evaluates Hessian Matrix.

Code A1.

```
clear all
clc
syms b n w h vf LAMBDA a r
theta = 1;
lambda1 = 3.7;
delta = .4;

s = [a; b; n; w; h;LAMBDA];
%Objective Function
H = (35.01-3.86*b-1.3734*n-.9574*h+62.78*vf);
%Volume Fraction Constrained Equation
g = (((2*(h-delta+lambda1))+a+((n-1)*(a-theta)))-(vf*(((a+(2*b))*h*w)-(2*(h-
delta+lambda1))+a+((n-1)*(a-theta)))))
F = H-(g*LAMBDA);

%First partial derivate
Pa = diff(F,a);
Pb = diff(F,b);
Pn = diff(F,n);
Ph = diff(F,h);
Pw = diff(F,w);
PLAMBDA = diff(F,LAMBDA)
PA = Pa;
PB = Pb;
PN = Pn;
PH = Ph;
PW = Pw;
PLAMBDA2 = PLAMBDA;

% Residual Matrix (7x1)
r = [PA; PB; PN; PH; PW; PLAMBDA2]

%Jacobian- Heissen Matrix
J = jacobian([r], [a, b, n, h, w, LAMBDA])
```

Appendix B

Code A2.

```
function s = lagrange_evaluation
syms b n w h vf LAMBDA a r theta lambda1 delta
%Parameters used for optimization
   m     = 0;          % Initialize in zero
   TOL   = 0.002;      % Tolerance
   max_m = 1000;       % max iterations

   %(initial guess)
   a      = 5;
   b      = .5;
   n      = 11;
   w      = 1;
   h      = 16;
   vf     = .9;
   LAMBDA = 2;

% Initialize residual matrix (7x1)

    r = [-LAMBDA*(n - vf*(n + h*w));
        2*LAMBDA*h*vf*w - 193/50;
        LAMBDA*(vf*(a - 1) - a + 1) - 6867/5000;
        LAMBDA*(vf*(w*(a + 2*b) - 2) - 2) - 4787/5000;
        LAMBDA*h*vf*(a + 2*b);
        vf*(a - 2*h + (a - 1)*(n - 1) + h*w*(a + 2*b) - 33/5) - 2*h - a - (a - 1)*(n - 1) - 33/5];

% while loop
   while ((norm(r) > TOL) && (m < max_m))

 J = [              0,            0,    LAMBDA*(vf - 1),            LAMBDA*vf*w,
LAMBDA*h*vf,        vf*(n + h*w) - n;
    0,           0,                0,          2*LAMBDA*vf*w,      2*LAMBDA*h*vf,
2*h*vf*w;
    LAMBDA*(vf - 1),          0,                0,                  0,                0,      vf*(a - 1) - a +
1;
    LAMBDA*vf*w, 2*LAMBDA*vf*w,                 0,                  0, LAMBDA*vf*(a +
2*b), vf*(w*(a + 2*b) - 2) - 2;
    LAMBDA*h*vf, 2*LAMBDA*h*vf,                 0,     LAMBDA*vf*(a + 2*b),                0,
h*vf*(a + 2*b);
    vf*(n + h*w) - n,     2*h*vf*w, vf*(a - 1) - a + 1, vf*(w*(a + 2*b) - 2) - 2,     h*vf*(a +
2*b),                  0]

% Solve for ds
      ds = -1*(J\r)
```

```
      % add ds to s ------ s = s + ds
      a      = a + ds(1);
      b      = b + ds(2);
      n      = n + ds(3);
      h      = h + ds(4);
      w      = w + ds(5);
      LAMBDA     = LAMBDA + ds(6);


% Recalculate r
  r = [-LAMBDA*(n - vf*(n + h*w));
        2*LAMBDA*h*vf*w - 193/50;
        LAMBDA*(vf*(a - 1) - a + 1) - 6867/5000;
        LAMBDA*(vf*(w*(a + 2*b) - 2) - 2) - 4787/5000;
        LAMBDA*h*vf*(a + 2*b);
        vf*(a - 2*h + (a - 1)*(n - 1) + h*w*(a + 2*b) - 33/5) - 2*h - a - (a - 1)*(n - 1) - 33/5];

      m = m + 1;
   end

% final values of s
   s = [a; b; n; h; w; LAMBDA]

% final results
   if ((m >= max_m) && (norm(r) > TOL))
      fprintf(1, 'WARNING: maximum number of iterations reached without a solution!\n');
      fprintf(1, 'Current solution...\n');
      fprintf(1, 'a = %4.4f\nb = %4.4f\nn = %4.4f\nw = %4.4f\n', a, b, n, w);
      fprintf(1, 'h = %4.4f\nvf = %4.4f\nLAMBDA = %4.4f', h, vf, LAMBDA);
   else
      fprintf(1, 'A solution was found after %d iterations!\n', m);
      fprintf('a = %4.4f\nb = %4.4f\nn = %4.4f\nw = %4.4f\n', a, b, n, w);
      fprintf('h = %4.4f\nvf = %4.4f\nLAMBDA = %4.4f', h, vf, LAMBDA);
   end
return
```

Appendix C

MATLAB code (.M file)

A MATLAB code (A3.) implemented to solve a constrained optimization problem using linear programming (lingprog) to find the optimal input variables.

Code A3.

```
clear all
clc
syms b n w h vf LAMBDA a r
theta = 1;
lambda1 = 3.7;
delta = .4;

%Objective Function:
h = [-.3417;-4.202;1.1331;-3.694;-1.246;-0.0180;0;0;0;0;0;0];
%Constraints:
% g(x) = 2*h - n + (28*vf)/5 + a*n + 2*h*vf + n*vf - a*n*vf - a*h*vf*w - 2*b*h*vf*w + 38/5
A = zeros(12,12);
b = zeros(12,1);
Aeq = [0 0 -1 0 2 (28/5) 1 2 1 -1 -1 -2;
   0 0 0 0 0 0 0 0 0 0 0 0;
   0 0 0 0 0 0 0 0 0 0 0 0;
   0 0 0 0 0 0 0 0 0 0 0 0;
   0 0 0 0 0 0 0 0 0 0 0 0;
   0 0 0 0 0 0 0 0 0 0 0 0;
   0 0 0 0 0 0 0 0 0 0 0 0;
   0 0 0 0 0 0 0 0 0 0 0 0;
   0 0 0 0 0 0 0 0 0 0 0 0;
   0 0 0 0 0 0 0 0 0 0 0 0;
   0 0 0 0 0 0 0 0 0 0 0 0;
   0 0 0 0 0 0 0 0 0 0 0 0];
beq = [-38/5;0;0;0;0;0;0;0;0;0;0;0];

lb = [5;.4;7;.73;14;7;0;0;0;0;0;0];
ub = [10;.8;25;1.27;17;10;0;0;0;0;0;0];

x = linprog(h,A,b,Aeq,beq,lb,ub);
```

Appendix D

Metal Sintering

7.1 Overview

In this section, a research opportunity in the field of Stainless Steel Power metallurgy and Sintering process is explained briefly. The powder metallurgy (PM) process, involves mixing metal powders, compacting the mixture in a mold, and then sintering, or heating, the resultant shapes in an atmosphere-controlled furnace to metallurgically bond the particles [50]. Sintering is described as the process where metal powder metals are transformed to solids by using temperatures below their melting point. During the sintering process, powder particles are bonded together by diffusion and other atomic transport mechanisms; thus, the porous solid acquires mechanical strength [51]. Powder metallurgy offers advantages in the process of forming materials. Sintering can form a dimensionally high precision, complex solid shapes in a single step. In other words, sintering often eliminates machining process. Reduced assemblies, since multiple parts and assembly steps are consolidated into a single PM component that minimizes manufacturing steps and reduces cost. Also, mechanical strength of sintered parts is increased since the final density approaches to a continuous solid [52]. The sintering process is governed by the following parameters:

- Temperature and time
- Geometrical structure of the powder particles
- Composition of the powder mix
- Density of the powder compact
- Composition of the sintering furnace

7.2 Powder Metallurgy of Stainless Steel

Stainless steel, a class of ferrous alloys, is well known for their resistance to corrosion, creep and high temperature applications. In fact, it is known that the resistance to oxidation as well

as resistance to creep at high temperatures by stainless steel are normally excellent as compared to other alloys [53]. Due to high increase in demand of powder metallurgy components made from stainless steel in variety of applications, including aerospace, automotive, biomedical field, among others; it has become of a great interest in the research domain [54].

Understanding of the proper processing techniques is critical in producing such components with significant properties and to extend the use of powder metallurgy technology for its considerable economic value of increasing number of applications. The following sections briefly describes the process of powder metallurgy and sintering.

7.2.1 Mold

The first step in creating a metal through powder metallurgy is to design a mold. It is important to consider shrinkage of the molded parts; since there is a decrease in size of approximately 20% when they are heated in a furnace during the sintering process [55]. For the mold design the measurements from the "Standard Test Method for Flexural Properties of Unreinforced and Reinforces Plastics and Electrical Insulating Materials by Four-Point Bending" was considered. The material chosen for the mold was steel due to its high strength. Then, the geometry was sketched in NX 8.5; and later machined in CNC milling machine. The following Figures 7.1 and 7.2 show the top and bottom part of the mold where the stainless-steel powder will be deposited

Table 7.1: Top and bottom mold dimensions (mm)

Mold	Length ($\boldsymbol{L}$) **mm**	Height ($\boldsymbol{H}$) **mm**	Width ($\boldsymbol{W}$) **mm**
Top	79.756	10.16	24.638
Bottom	80.264	7.62	25.146

Figure 7.1: Top part of the mold

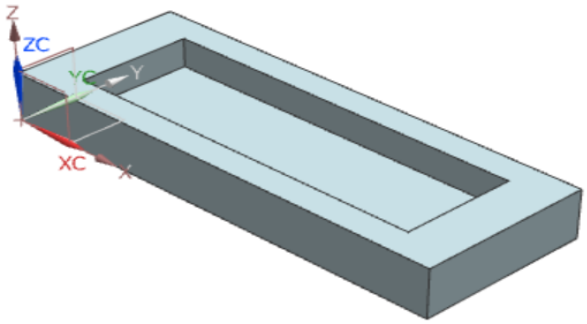

Figure 7.2: Bottom part of the mold

7.2.2 Stainless Steel Pre-Processing

7.2.2.1 Stainless Steel Powder Mixture

The 316 L Stainless steel powder mixture was prepared for this research as follows: The micro powder (Alfa Aesar) with an average size ranging from -40 to +80 mesh. The binder employed to prepare the feedstock ($\mathbf{60\%\ Stainless - Steel\ Powder\ + 40\%\ Binder}$) was composed of paraffin wax. The feedstock was mixed until fully blended. The desired thickness of the specimen according to the ASTM standards mentioned in 7.2.1 is 2.28 mm. To achieve this, 19.89 grams of feedstock are needed to fill $\mathbf{4.43}\ \boldsymbol{cm^3}$ of the bottom mold. Then, the mixture was deposited into the mold at room temperature under the pressure of 30, 000 $\frac{\boldsymbol{N}}{\boldsymbol{m^2}}$ using the Instron 5969 under compression testing. Because of an applied high pressure, the powder will turn into a "green compact." as is comes out of the steel mold. The compact has the size and shape of the finished product. The strength of the compact is just sufficient for in the careful handling and transportation to the sintering furnace.

7.2.2.2 Stainless Steel Sintering Temperature

The next stage in the production of powder metal stainless steel is called sintering. As mentioned in section 7.1, sintering is defined as "The thermal treatment of a powder or compact at a temperature below the melting point of the main constituent, for the purpose of increasing its strength by bonding together of the particles." [55]. To achieve this, a specially designed furnace with the capability of having a controlled atmosphere is used. In these type of furnaces, the "green compacts" are brought to a temperature just below the stainless-steel melting point. For 316L Stainless-steel, this temperature is approximately 1400-1450 °C.

Sintering process can be divided in different stages. The stage of sintering, impurities and binder materials (Paraffin wax) are melted or removed. Then, to prevent oxidation of the metal powder, an argon atmosphere is created inside the furnace. As the part approaches the stainless-steel melting temperature a process called solid state bonding occurs forming a solid metal part. It is important that the temperature not go above this point or the part may melt. [54].

7.2.3 Process and Results

The stainless-steel "green compacts" were subjected to heat treatments of debinding and sintering. In the debinding process, the molded parts were heated to 400 °C for 1 hour in an argon atmosphere argon (Ultra high purity 99.99%) at different heating rates of 3 to 10 °C/min. After the debinding process, the sintering process was carried out in different ways by heating up from 400 °C to different temperatures and different sintering times.

Table 7.2 shows in detail the sintering temperatures as well as the results obtain at each temperature and sintering time. Empirical evidence showed that, when using temperatures above 1300 °C powder metals achieve a fully solid state. However, stainless-steel specimen loses its shape due to the melting of the metal. Also, in temperatures ranging from 1300 °C to 1360 °C, Widmannstätten structure or needle patterns were formed in the specimen due to the overheating of the stainless-steel powder as observed in Figure 7.3

Figure 7.3: Stainless-Steel sintered at 1360 °C for 5 hours

In addition, several specimens that were sintered at temperatures ranging from 1250 °C to 1230 °C, demonstrated that these temperatures are the boundaries between melted or brittle specimens as observed in the table below. Even though some of the specimens were melted at these temperatures, they also showed low strength properties as shown in Figure 7.4

Figure 7.4: Stainless-Steel sintered at 1250 °C for 1 hour

For this reason, a specimen was sintered for 24 hours at a temperature of 1225 °C to see if sintering time has an impact over the strength of the specimen. Best results were obtained at this sintering time, the specimen increased its strength properties and did not lose shape. As it is observed in the table, small (ΔT) changes in temperature *i.e.* 1230 °C to 1228 °C shows huge difference between a brittle specimen and a melted specimen. However, if the sintering time is increased in the temperatures ranges where specimens are brittle, the strength is increased. Therefore, the proposed time and temperature for the stainless steel "green compacts" is 1228 °C for 24 hours to see how the strength is increased from 1225 °C for 24 hours to 1228 °C for 24 hours.

Table 7.2: Sintering Temperatures, time and results for Stainless-Steel specimens

Sintering Temperature (Celsius)	0.5 hours	1 hour	5 hours	7 hours	24 hours
1360	Melted	Melted	Melted	-	-
1300	Melted	Melted	Melted	-	-
1250	Melted	Melted	Melted	-	-
1230	Brittle	Melted	Melted	Melted	-
1228	Brittle	-	-	-	Proposed Temp and time
1225	Brittle	Brittle	Brittle	-	Sintered (Brittle)
1200	Brittle	Brittle	-	-	-

Vita

Tania Alejandra Ventura Luna was born in 1992 in Celaya, Guanajuato, Mexico. She is the youngest of three daughters of Raul and Rosa. She completed her high school education at Colegio Manuel Concha “Marista” located in Celaya, Guanajuato, Mexico in June 2010. In the fall of that year, she enrolled at The University of Texas at El Paso and graduated in May 2015 with the B.S degree in Mechanical Engineering. Upon graduation, she immediately enrolled for graduate studies to pursue a M.S degree in Mechanical Engineering. In spring 2015, she obtained a research assistant position with Dr. Jack F. Chessa.

Contact Information: <taventuraluna@miners.utep.edu>

This thesis/dissertation was typed by <Tania Alejandra Ventura Luna>.